Calcium Isotopic Compositions of Neogene Dolomites in the South China Sea and Its Implications for Paleoclimate Changes

X. F. Liu[1,2], X-M. Liu[2*], S. K. Zhai[1*], C. Cao[2], D. J. Bi[3], X. Y. Liu[4], Z. F. Zhang[5]

[1]College of Marine Geosciences, Ocean University of China, Qingdao, China, [2]Department of Geological Sciences, University of North Carolina, Chapel Hill, NC, USA, [3]First Institute of Oceanography, Ministry of Natural Resources, Qingdao, China, [4]Zhanjiang Branch Institute of China National Offshore Oil Corporation Limited, Zhanjiang, China, [5]State Key Laboratory of Isotope Geochemistry, Guangzhou Institute of Geochemistry, Chinese Academy of Sciences, Guangzhou, China

Corresponding author: Xiao-Ming Liu (xiaomliu@unc.edu); Shikui Zhai (zhai2000@ouc.edu.cn)

Key Points:

- Pure XK-1 dolomites forming in seawater-like fluid-buffered diagenetic environments can fully record the Ca isotopic composition of primary paleo-seawater
- The Ca isotope fractionation factor between XK-1 dolomites and seawater ($\Delta^{44/40}Ca_{dol\text{-}sw}$) is constant, which is inferred to be between -0.5 and -0.8‰
- Enhanced continental weathering and global cooling may have driven more CO_2 to be sequestered by pelagic carbonate burial

Abstract

Marine carbonates, including shallow-water carbonates and pelagic carbonates, precipitating from seawater and representing the largest sink of calcium (Ca) and carbon (C) at Earth's surface, could record seawater chemistry. Therefore, marine carbonates help regulate atmospheric carbon dioxide (CO_2) concentration and eventually Earth's long-term climate change. Calcium stable isotope geochemistry is a powerful tool to reconstruct paleo-seawater Ca isotopic compositions ($\delta^{44/40}Ca_{sw}$) and to constrain the global Ca and C cycles over geological history. Here, we present a Neogene record of $\delta^{44/40}Ca$ from pure dolomites of the core XK-1 in the South China Sea. We propose that the dolomites formed in seawater-like fluid-buffered diagenetic environments near the seawater-sediment interface. We demonstrate that XK-1 dolomites display no Ca isotope fractionation from seawater, and hence may serve as good archives of contemporaneous seawater $\delta^{44/40}Ca$. Further, we quantify respective contributions of shallow-water and pelagic carbonates in sequestering carbon over the Neogene, using a Ca isotope mass balance box model. We find that more CO_2 may have been sequestered by pelagic carbonate burial during global cooling. The enhanced continental weathering, global cooling, sea-level fall, seawater chemical changes, and pelagic carbonate burial are tightly linked.

Plain Language Summary

At Earth's surface, terrestrial weathering could consume carbon dioxide (CO_2) and bring calcium (Ca) ion into the ocean via riverine delivery, and help regulate the atmospheric CO_2 change and climate. Therefore, the Ca cycle is tightly linked to the carbon cycle. When calcium ions and carbonate ions meet in the ocean, they will combine through a chemical reaction to form a new mineral called calcium carbonate ($CaCO_3$), which later become carbonates. As a result, marine carbonates could record their precipating seawater chemistry. Our work aims to reconstruct changes in the Ca isotopic composition ($\delta^{44/40}Ca$) in the ocean over the Neogene, and to quantitatively constrain the distribution of the carbonate accumulation sequestering CO_2 over the Neogene. We find that pure dolomites of the core XK-1 in the South China Sea formed in seawater-like fluid-buffered diagenetic environments near the seawater-sediment interface, and hence may be good archives of contemporaneous seawater Ca isotopic composition ($\delta^{44/40}Ca_{sw}$). In addition, we quantify respective contributions from shallow-water and pelagic carbonates in sequestering CO_2 over the Neogene, using a Ca isotope mass balance box model. We find that enhanced continental weathering and global cooling may have driven more CO_2 to be sequestered by pelagic carbonate burial, which also influences the seawater chemical changes. Our work improve the understanding of past variations in seawater chemistry and climate change.

1 Introduction

Carbonate rock ($CaCO_3$ or $CaMg(CO_3)_2$) as a common type of sedimentary rock directly precipitated from seawater is not only an important archive of seawater chemistry, but also a dominant removal path for CO_2 from Earth's surface on geological time scales. The Ca and C cycles in global ocean is controlled by weathering, hydrothermal activity, and carbonate precipitation and dissolution (Farkaš, 2018; Husson et al., 2015). Hence, the Ca cycle of the ocean is fundamentally linked to the atmospheric CO_2 change and therefore influenced by long-term climate change (Berner & Berner, 1997; Elderfield, 2010; Urey, 1952).

The stable Ca isotope proxy ($\delta^{44/40}Ca$) of Ca-bearing minerals has become a powerful tool to reconstruct paleo-seawater Ca isotope signatures and to constrain the oceanic Ca cycle over Earth history based on different archives since the origins of mass spectrometry (Griffith et al., 2020; Griffith & Fantle, 2020; Gussone et al., 2020). For example, late Cenozoic records of seawater $\delta^{44/40}Ca$ values ($\delta^{44/40}Ca_{sw}$) have been generated from various sedimentary archives, including bulk carbonate sediments (Fantle & DePaolo, 2005, 2007; De La Rocha & DePaolo, 2000), foraminifera (Heuser et al., 2005; Sime et al., 2007), barites (Griffith et al., 2008), phosphates (Arning et al., 2009; Schmitt et al., 2003), and corals (Gothmann et al., 2016). Large differences in $\delta^{44/40}Ca_{sw}$ inferred from these archives probably indicate the effects of both diagenesis and variability in the Ca isotope fractionation factors between Ca-bearing minerals and seawater. Here we summarize previous investigations of Ca isotope fractionation as follows. For inorganic carbonates, $CaCO_3$ mineralogy (Gussone et al., 2005), mineral precipitation rate and saturation state (AlKhatib & Eisenhauer, 2017; DePaolo, 2011; Fantle & DePaolo, 2007; Gussone et al., 2005; Lemarchand et al., 2004; Nielsen et al., 2012; Tang et al., 2008), and $CaCO_3$ stoichiometry (Harouaka et al., 2014; Nielsen et al., 2012) all affect Ca isotope fractionation. For example, ~2‰ fractionation of $\delta^{44/40}Ca$ for calcite was discovered at different conditions, while temperature has little effect (generally <0.02‰/°C, as compiled in Gussone and Heuser, 2016). By contrast, the parameters controlling the Ca isotope fractionation of inorganic carbonates have little effect on that of biogenic carbonates such as corals, coccolithophores, and foraminifers (Inoue et al., 2015; Kısakürek et al., 2011; Langer et al., 2007; Roberts et al., 2018). This observed isotope fractionation in biogenic carbonates is probably caused by different cellular Ca transport pathways (Gussone et al., 2006). Due to the inherent species-specific Ca isotope fractionation, biominerals become appropriate archives for the $\delta^{44/40}Ca_{sw}$ reconstruction (Sime et al., 2007). However, one possible limitation is that the availability of easily calibrated archives. As calibrations of the fractionation coefficient are based on the culture experiments of modern species and samples collected from the modern environments, we need to identify suitable archives for the relatively recent carbonates but probably not for ancient carbonates in geological records (Gussone et al., 2020). Diagenesis is another main limitation in using marine bulk inorganic or biogenic carbonates to reconstruct the Ca cycle evolution through time. Diagenesis is ubiquitous in bulk carbonates after they are buried and the geochemical indices actually reflect signals of diagenesis (Fantle et al., 2020; Swart, 2015). Recent foraminifera studies have shown that even carbonate skeletal biominerals that are usually assumed to be pristine and geochemically resilient may have been influenced by diagenetic alterations (Bernard et al., 2017; Chanda et al., 2019; Kozdon et al., 2018).

Early diagenetic dolomites may serve as good archives of seawater chemistry and are important Ca budget to construct the global Ca cycle. For example, Li et al. (2015) and Hu et al. (2017) proposed that massive syn-depositional dolomites probably record Mg isotopic compositions of coeval seawater. Ahm et al. (2018) and Higgins et al. (2018) emphasized the utility of using paired measurements of Ca and Mg isotopes and numerical modeling approaches to identify whether sediment-buffered or fluid-buffered dolomitization dominates and suggested that dolomites formed under fluid-buffered (specifically seawater-buffered) conditions should be a reliable archive of ancient seawater chemistry. Previous studies showed that it is possible to obtain the chemical composition of the dolomitizing fluid (glacial seawater) using numerical diagenetic modeling of $\delta^{44/40}Ca$ values versus Sr/Ca ratios, $\delta^{26}Mg$, $\delta^{13}C$ and $\delta^{18}O$ isotopes (Ahm et al., 2018, 2019). Moreover, Tostevin et al. (2019) investigated the possibility of Ca isotopes as a record of the marine Ca cycle versus carbonate diagenesis during the late Ediacaran. They

concluded that $\delta^{44/40}Ca$ variations preserved in ancient carbonate rocks are probably linked to enhanced continental weathering, increases in evaporite deposition, and changes in the style of dolomitization. In addition, Chang et al. (2020) used clumped-isotope temperature ($T_{\Delta47}$) records to constrain a suite of Ediacaran massive dolomites with low-temperature origin. Combined with cogenerated elemental, isotopic, and petrographic data, they confirmed that dolomites formed in an early diagenetic environment with seawater-derived fluids and abundant microbial activity could be faithful recorders of early ocean chemistry. In sum, previous studies demonstrated that dolomites formed in the fluid-buffered diagenetic environment could be a promising archive of paleo-seawater chemistry.

Here, we present Ca isotopic composition ($\delta^{44/40}Ca$) records in dolomites from the well XK-1 in the Xisha Islands of the South China Sea from the Neogene to the present. Using paired Ca and Mg isotope approach, combined with coexisting elemental, Sr-C-O isotopic, fluid inclusion chemical and petrographic data, we identified these dolomites produced by seawater-buffered dolomitization. Therefore, we reconstruct $\delta^{44/40}Ca_{sw}$ variations since the Neogene using Ca isotopic composition in dolomites ($\delta^{44/40}Ca_{dolomite}$). Further, we use a steady-state mass balance model for seawater $\delta^{44/40}Ca$ over the late Cenozoic to constrain the relative flux changes of the two main Ca sinks, i.e., shallow-water carbonates and pelagic carbonates, providing independent estimates for $\delta^{44/40}Ca_{shallow}$ (calculated from $\delta^{44/40}Ca_{dolomite}$) and $\delta^{44/40}Ca_{pelagic}$ (seen as $\delta^{44/40}Ca_{bulk\ nannofossil\ ooze}$ from De La Rocha and DePaolo (2000), Fantle and DePaolo (2005), and Fantle and DePaolo (2007)). According to the model result, we discuss the relationship among continental weathering, climate change, sea-level fluctuation, seawater chemistry, and carbonate burial.

2 Geological setting and samples

The Xisha Islands (15°43′-17°07′ N, 111°11′-112°54′ E, Fig. 1a), also known as the Paracel Islands, are located on the northwestern continental slope of the South China Sea (SCS). The archipelago includes more than 40 islands and reefs, with a maritime area of around 1.5×10^4 km^2 and a land area of approximately 8 km^2 (He & Zhang, 1986). The Xisha carbonate platform with a thickness of approximately 1250 m lies on a uplifted basement (i.e. the Xisha Uplift) composed of the Precambrian granite gneisses and Mesozoic granites (Fig. 1b) (He & Zhang, 1986; Wang et al., 1979; Xiu et al., 2016; Zhu et al., 2017). The tectonic subsidence of the Xisha area initiated in the Oligo–Miocene transitional period caused by the seafloor spreading and regional crustal stretching in the SCS (Mathew et al., 2020; Wu et al., 2016). Since then, the Xisha Uplift has sunk below sea level and been gradually subsiding due to subsequent post-rifting thermal subsistence which was ubiquitous along the northern margin of the SCS (Fig. 1c) (Lü et al., 2013; Wang et al., 2014; Wu et al., 2014). As a result, the Xisha carbonate platform has been successively growing from the Miocene to the present and is now surrounded by basins or depressions with a unified water depth of over 1000 m (Wu et al., 2014).

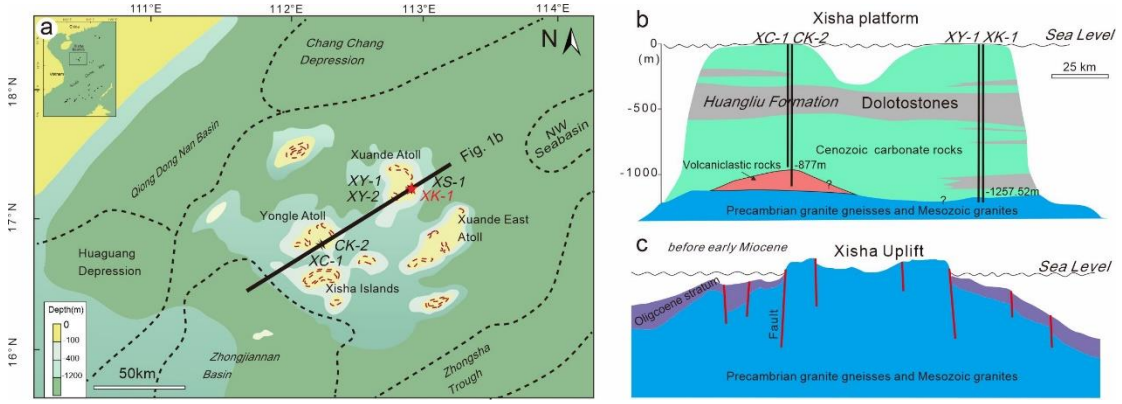

Fig. 1. Location of the Xisha Islands, well XK-1 and other wells drilled in the studied area, modified from Wang et al. (2018).

In the past five decades, a total of six wells in the Xisha Islands have been drilled for scientific research. They are Xiyong-1 (XY-1, 1384.68 m deep), Xichen-1 (XC-1, 802.17 m deep), Xiyong-2 (XY-2, 600.02 m deep), Xishi-1 (XS-1, 200.63 m deep), Xike-1 (XK-1, also named ZK-1, 1268.02 m deep), and Chenke-2 (CK-2, 928.75m deep), respectively (Fig. 1a) (Bi et al., 2018a; Fan et al., 2019; Zhao, 2010). Based on detailed stratigraphic studies of these wells, the carbonate platform strata are divided into five formations including the Sanya, Meishan, Huangliu, Yinggehai, and Ledong formations, which correspond to the Early Miocene, Middle Miocene, Late Miocene, Pliocene, and Quaternary respectively (Wu et al., 2014; Zhao, 2010). Among these wells, the XK-1 and CK-2 wells provide ideal carbonate cores as they penetrate through the entire Neogene carbonate succession with average core recovery rates of higher than 80% and 70%, respectively. Importantly, the well XK-1 not only penetrates the thick carbonate section (0–1257 m), but also reaches around 10 m below the basement (1257–1268 m). Moreover, previous studies have established a basic geochronological framework for the well XK-1 based on magnetostratigraphic and biostratigraphic data (Wu et al., 2019; Yi et al., 2018) (Fig. 2). The age of the bottom boundary (1257.4 m) for the well XK-1 carbonate succession is 23 Ma. The ages of two unconsolidated sections at the depths of from 1050 to 795.74 m and from 760 to 632 m, respectively, are undetermined due to lack of effective palaeomagnetic and biostratigraphic constraints. Detailed data for the age model can be found in Wu et al. (2019) and references therein.

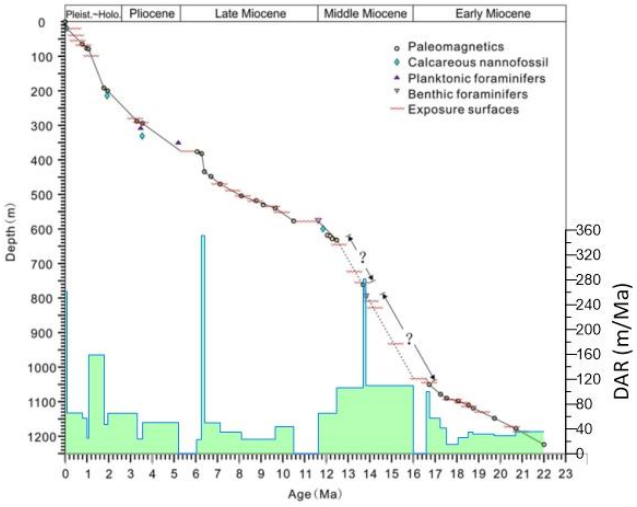

Fig. 2. Age-depth model for the core XK-1, modified from Wu et al. (2019). DAR denotes the depositional accumulation rate of the XK-1 carbonate sediments, which is calculated based on the control point data of the age-depth model.

Detailed descriptions of the sedimentology, mineralogy, and geochemistry for the core XK-1 have been published in the past five years (Bi et al., 2018a; Bi et al., 2018b; Bi et al., 2019; Shao et al., 2017; Wang et al., 2018; Wu et al., 2019; Zhai et al., 2015) and are only briefly described here. The core XK-1 is mostly composed of carbonate minerals, including aragonite, high-magnesium calcite (HMC), low-magnesium calcite (LMC), and dolomite, with an average content percentage of 2.5%, 1.4%, 66%, and 29%, respectively (Fig. 3). Within top 35.4 m, the core consists of aragonite, HMC and LMC, of which the average content is 30%, 19% and 51% respectively. Below 35.4 m, HMC disappears, aragonite sporadically distributes at depth of 207~230 m, 306.3 m, 387 m, and 445.6 m, and LMC and dolomite alternately appear, which are two major carbonate components throughout the whole core. Between 0 and 1200m, four calcite layers and seven dolomite layers have been identified. At the bottom (1211~1257.4 m), there exist a small amount of terrigenous minerals composed of feldspar, quartz, kaolinite, smectite, and mica. Their total abundance ranges from 0 to 100%, with an average value of 25%.

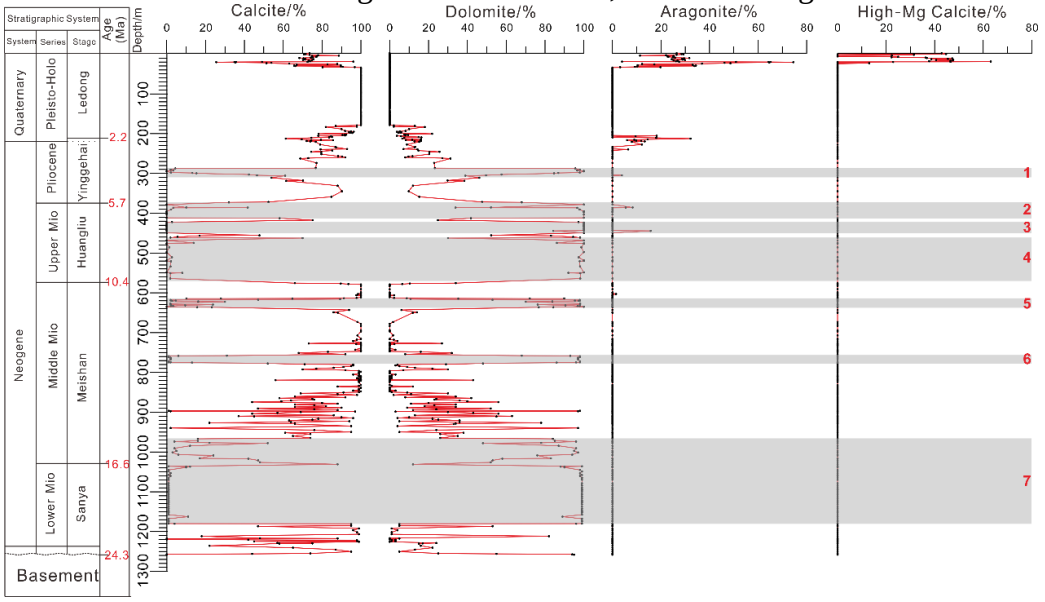

Fig. 3. Mineral compositions of the core XK-1, data from Xiu (2016) and Zhai et al. (2015). The gray band represents the dolomite layer. Seven layers have been identified in total.

Various diagenesis processes are described below. (1) Meteoric diagenesis: The upper 180 m is affected by meteoric diagenesis as subaerial exposure surfaces occur frequently and unstable minerals including primary aragonite and HMC are transformed to be pure LMC. Negative $\delta^{13}C$ and $\delta^{18}O$ values found in samples of this section could be attributed to the influence of the meteoric fluids. During sea-level low stands, both oxidation of organic matter with isotopically light carbon and addition of meteoric water with isotopically light oxygen contribute to the chemical composition of carbonate minerals. (2) Marine burial diagenesis: All depths below the upper meteoric zone have mostly undergone marine burial diagenesis, which includes $CaCO_3$ cementation, recrystallization, and polymorphic transformations. In this lower interval, except for the fibrous aragonites formed by cementation instead of protogenetic processes in the interval of 207~242 m (Zhai et al., 2015), all primary aragonite and HMC are converted into the more thermodynamically stable LMC. Positive $\delta^{13}C$ values and gradually

increased $\delta^{18}O$ values with depth of samples in this section also indicate the effect of marine burial diagenesis. (3) Dolomitization: The core XK-1 contains both massive and partially dolomitized stratigraphic intervals and is characterized by two ~200-m-thick dolomite layers that are 100% dolomitized (370~565 m and 966~1180 m, respectively) (Fig. 3). In total, seven dolomite sub-layers with various thicknesses developed from the Early Miocene to the Pliocene throughout the whole core. Regionally, ~20-m-thick and ~200-m-thick dolomite layers formed during the Pliocene and the Miocene can also be found in the XY-1, XY-2, XC-1, and CK-2 wells. This indicates that the development of the Xisha dolomite layer is at least a regional event rather than a local event. In addition to the Xisha area, Neogene dolomites are widespread worldwide, indicating that their formation may be controlled by globally unified paleoclimate and paleo-ocean conditions (Budd, 1997; Fouke et al., 1996; Meyers et al., 1997; Pleydell et al., 1990; Ren & Jones, 2017). The frequent and widespread occurrence of exposure surfaces demonstrates that the formation of massive dolomites is related to the decline of relative sea level. Considering that the core XK-1 is located on the edge of the isolated Xisha carbonate platform, the dolomitization process should occur under fluid-buffered diagenetic conditions with a dolomitizing fluid most similar to seawater, which is supported by our latest Ca and Mg isotope evidence (refer to discussion section 5.1).

Here we selected 18 dolomite samples from the core XK-1 for mineralogical, elemental and Ca isotope analyses based on the principle of equidistant sampling, or to be precise, based on the principle of equal-time sampling. All chosen samples have dolomite content higher than 95%, mostly up to 100%. Sampling details including depth, age, and mineral content are listed in Table 1 and shown in Fig. 3.

3 Analytical methods

3.1 Mineralogical analyses

Mineralogical analyses were carried out on a Bruker D8 Advance X-ray diffractometer (XRD) in the Open Laboratory, Qingdao Institute of Bioenergy and Bioprocess Technology, Chinese Academy of Sciences. The powder samples were generally flattened on the sample table, followed by XRD measurements using a rotating Ni-filtered Cu anode X-ray source (λ = 0.15406 nm), operated at 40 kV and 40 mA with a 2θ step scan of 0.030° and a scanning rate of 4° 2θ/min. Data were processed using MDI Jade 6.5 software. The relative percentages of dolomite and calcite were calculated based on the (104) peak intensity value of the two minerals (Royse et al., 1971). Dolomite stoichiometry was calculated using the d (104) value (Jones et al., 2001). The degree of cation ordering in dolomite was calculated according to the intensity of the (015) and (110) peaks, i.e. I (015/110) values, where I represents the intensity.

3.2 Ca isotopic measurements

Leaching and digestion of carbonate components, purification of Ca element, and instrumental analysis of Ca isotopes were performed at the State Key Laboratory of Isotope Geochemistry, Guangzhou Institute of Geochemistry, Chinese Academy of Sciences, following the procedure described in Zhu et al. (2016, 2018) and Liu et al. (2017). The procedure is briefly described here.

Approximately 30 mg of sample powders were weighed and dissolved in 1 mL 0.9 N HNO_3. Reacting for about 0.5 h to ensure complete dissolution of the carbonate components. The

resulting solutions were centrifuged for 10 mins at 6000 rpm. Centrifugation can separate the non-carbonate residue from the carbonate supernatant. Then, the supernatant was re-dissolved in 0.5 mL concentrated HNO_3 for several times. Finally, the dried sample was dissolved in 1.5 mL of 1 N HNO_3 for Ca element purification. The protocol for Ca purification is as follows. First, an aliquot of sample solution containing 30 μg of Ca was mixed with the ^{42}Ca-^{43}Ca double spike solution in an appropriate amount. The mixture was dried down and re-dissolved in 0.1 ml of 1.6 M HCl for column chemistry. Then, the re-dissolved mixture was loaded onto a Teflon microcolumn filled with 1 ml of AG MP-50 (100–200 mesh) resin and eluted with 1.6 M HCl continuously, during which Ca was gradually isolated from the sample matrix. The Ca yield rate was generally higher than 99%. To access the reproducibility and quality, one replicate sample, one reference material and one blank were processed as unknowns for every twelve samples. The total Ca amount of procedure blanks were less than 25 ng, which were negligible compared to 30 μg of Ca loaded onto the column.

Ca isotopic compositions were measured on a Trition^{TM} Thermal Ionization Mass Spectrometry (TIMS). The ^{41}K was monitored to correct the isobaric interference of ^{40}K on ^{40}Ca using $^{40}K/^{41}K = 1.7384 \times 10^{-3}$ (Heuser et al., 2002). To calibrate instrumental fractionation, a ^{42}Ca-^{43}Ca double spike technique using an iterative algorithm with an exponential law was utilized. For each sample, the same purified Ca cut was measured at least 3 times with different loaded filaments. All Ca isotope data are reported relative to NIST SRM 915a, that is, $\delta^{44/40}Ca = [(^{44}Ca/^{40}Ca)_{sample}/(^{44}Ca/^{40}Ca)_{SRM\ 915a} - 1] \times 1000$. The values of $\delta^{44/40}Ca$, two standard deviation (2SD) and two standard deviation of the mean (2SE) are reported in Table 1. The average $\delta^{44/40}Ca$ value of NIST SRM 915a and IAPSO seawater in this study are -0.02 ± 0.11‰ (2SD, n = 42) and 1.81 ± 0.11‰ (2SD, n = 46) respectively, consistent with previous studies within analytical uncertainty (e.g., Amini et al., 2009; Farkaš et al., 2007a, 2007b; Feng et al., 2018; He et al., 2017; Huang et al., 2010; Liu et al., 2017b; Valdes et al., 2014). In addition, one replicated sample (SCS-17) has less than 0.06‰ offset, which show high reproducibility within uncertainty.

4 Results

The depth of XK-1 dolomite samples is between ~289 and 1180 m and the depositional age is from ~0.4 to 21 Ma. Our mineralogical, Ca isotopic data, together with previously published elemental concentrations of Al, Mn, Fe, Sr, as well as Sr, C and O isotopic data in bulk samples are provided in Table 1.

4.1 Mineralogy and elemental geochemistry

In the core XK-1, limestone and dolomite are interbedded. Seven dolostone layers and five limestone layers have been identified (Xiu, 2016; Zhai et al., 2015). X-ray diffraction (XRD) analyses indicate that all carbonate samples are mainly composed of pure dolomite, of which the content is greater than 95%, mostly reaching 100%, whereas the remaining mineral component is calcite. The parameter I (015/110) of dolomite cation ordering is calculated according to the intensity of peaks (015) and (110) in dolomite. It ranges from 0.27 to 0.90, with an average of 0.50. We determine the Ca/(Ca+Mg) molar ratio based on our XRD data using the Lumsden equation. The equation is expressed as: Ca/(Ca+Mg)=(md+b)/100, where d is observed d (104) value, m=333.33, and b=-911.99 (Jones et al., 2001; Lumsden, 1979). The calculated ratio varies from 0.53 to 0.57, with an average of 0.55. The results are consistent with previous published

elemental content data. The dolomite stoichiometry suggest that XK-1 dolomites are calcic dolomite [$Ca_{1.14\text{-}1.06}Mg_{0.86\text{-}0.94}(CO_3)_2$]. Al concentrations are low throughout the dataset, indicating that detrital contamination of all samples is negligible (Kamber et al., 2004). Low Mn and Fe concentrations, mostly lower than 50 and 400 ppm, respectively, suggest that additional late fluids like hydrothermal inputs, are not important. Our Sr content as well as Sr, C, and O isotopic data compare well with those of other pure dolomite such as the Bahamian dolomites (Higgins et al., 2018).

4.2 Ca isotopic composition ($\delta^{44/40}$Ca values)

The $\delta^{44/40}$Ca values of XK-1 dolomites vary between 1.08‰ and 1.35‰, with an average value of 1.22‰ relative to the NIST SRM 915a standard (Table 1). The variation of $\delta^{44/40}$Ca values has no correlation with age or lithology. The variation of $\delta^{44/40}$Ca over time in dolomite is almost consistent with that of planktonic foraminifera (Heuser et al., 2005). And the $\delta^{44/40}$Ca variation in dolomite is opposite to that of pelagic carbonates, which is mainly composed of nannofossil oozes (Fantle & DePaolo, 2005, 2007; Fantle & Higgins, 2014) (see 5.2 for details). The average $\delta^{44/40}$Ca value of XK-1 dolomite (1.22‰) is significantly higher than the mean $\delta^{44/40}$Ca value of carbonates measured over all geological historical time (0.61‰) and that of bulk nannofossil oozes over the past 35 Ma (~0.7‰).

Table 1. Measured $\delta^{44/40}$Ca values and previously published mineralogical and geochemical data of carbonates from the core XK-1

Sample	Depth m	Age Ma	Dolomite %	Calcite %	d (104)	I (015/110)	Al %	Mn μg/g	Fe %	Sr μg/g	Ca/(Ca+Mg) mmol/mol	$^{87}Sr/^{86}Sr$	$\delta^{13}C$ ‰	$\delta^{18}O$ ‰	$\delta^{44/40}Ca$ ‰	2SD ‰	N
SCS-1	289.3	3.8	100	0	2.91	0.27	0.03	14	0.01	280	0.57	0.709276	2.3	4.4	1.16	0.02	3
SCS-2	392.1	6.1	100	0	2.91	0.38	0.10	64	0.10	190	0.57	0.709135	2.4	5.3	1.30	0.01	3
SCS-3	404.7	6.4	100	0	2.90	0.44	0.02	7	0.01	186	0.55	0.709069	2.8	4.6	1.23	0.06	3
SCS-4	436.6	7.1	100	0	2.90	0.53	0.01	42	0.01	180	0.55	0.708998	2.9	4.6	1.22	0.12	3
SCS-5	489.9	8.4	100	0	2.90	0.45	0.03	22	0.02	188	0.53	0.709055	2.6	4.0	1.16	0.10	3
SCS-6	504.8	8.7	100	0	2.90	0.31	0.01	8	—	254	0.55	0.708909	3.0	2.8	1.30	0.16	3
SCS-7	528.8	9.3	100	0	2.90	0.41	0.01	7	—	186	0.55	0.708944	3.0	4.3	1.16	0.13	3
SCS-8	549.8	9.8	100	0	2.90	0.56	0.02	15	0.01	189	0.54	0.709104	3.2	5.3	1.34	0.01	3
SCS-9	630.4	11.1	100	0	2.90	0.41	0.01	9	0.01	208	0.56	0.708998	3.6	4.8	1.14	0.09	3
SCS-10	767.7	13.0	100	0	2.90	0.69	0.01	13	0.01	186	0.54	0.708952	3.5	4.7	1.24	0.03	3
SCS-11	896.7	14.8	100	0	2.90	0.56	0.01	9	0.01	157	0.56		2.9	5.1	1.22	0.08	3
SCS-12	973.8	15.8	96.3	3.7	2.90	0.90	0.03	15	0.03	186	0.55	0.708873	2.7	4.3	1.26	0.07	3
SCS-13	1006.8	16.3	94.9	5.1	2.90	0.55	0.03	16	0.02	178	0.56	0.708968	2.4	4.2	1.32	0.06	3
SCS-14	1064.6	17.5	99.3	0.7	2.90	0.52	0.03	73	0.03	181	0.55	0.709004	2.9	4.5	1.35	0.11	3
SCS-15	1094.8	18.4	99.4	0.6	2.89	0.37	0.05	32	0.03	183	0.53	0.708983	3.6	4.8	1.25	0.10	3
SCS-16	1112.0	18.9	98.4	1.6	2.90	0.49	0.03	24	0.01	183	0.54	0.708562	2.8	2.0	1.11	0.06	3
SCS-17	1137.0	19.6	100	0	2.90	0.51	0.01	14	—	191	0.55	0.708565	3.1	2.1	1.11	0.11	3
SCS-18	1179.5	20.8	100	0	2.91	0.57	0.12	54	0.08	233	0.57	0.708606	2.9	2.6	1.08	0.05	3

Note: (1) Age data calculated based on an age-depth model from Wu et al. (2019); (2) Mineralogical and Ca isotopic data from this study; (3) Elemental data from Bi et al. (2019) and Xiu (2016); (4) Sr isotopic data from Bi et al. (2018); (5) C and O isotopic data from Bi (2019); (6) C and O isotopic data are on V-PDB scales, Ca isotopic data on NIST SRM 915a scales; (7) N denotes number of measurements; (8) "—" means below detection limit; (9) 2SD represents two standard deviations.

5 Discussion

We first confine that XK-1 dolomites formed under seawater-like fluid-buffered diagenetic conditions. Therefore, they can be regarded as primary minerals, although they were diagenetically precipitated near the seawater-sediment interface via recrystallization from metastable precursor minerals. Then, we discuss the factors that may control the fractionation of Ca isotopes during marine dolomitization and elucidate that XK-1 dolomites can record the contemporaneous seawater chemistry. Further, we quantify the relative fluxes between shallow-water carbonates and pelagic carbonates in sequestering carbon during the Neogene, based on a Ca isotope mass balance box model. Finally, we elucidate the long-term relationship between continental weathering, climate change, sea-level fluctuation, seawater chemistry, and carbonate burial.

5.1 The effects of seawater-like fluid-buffered dolomitization on XK-1 dolomite formation

5.1.1 Seawater-like fluid-buffered dolomitization

Early marine diagenesis is ubiquitous in shallow-water marine carbonate sediments, which is generally associated with the transformation from unlithified metastable carbonate polymorphs, such as HMC and aragonite, into diagenetically stabilized minerals, namely, LMC and dolomite (Higgins et al., 2018; Melim et al., 2002). A fluid-buffered diagenetic system, which involves mass fluxes between local diagenetic fluids and sediments and is capable of significantly altering and in some cases completely resetting the chemical and isotopic composition of the primary sediment, is defined as one where the chemical composition of diagenetic minerals largely represents the chemical composition of the diagenetic fluid (Fantle & Higgins, 2014; Higgins et al., 2018). Two key processes are crucial in creating a fluid-buffered diagenetic environment. They are (1) slow sedimentation rate or depositional hiatus, and (2) continuous fluid flow, respectively (Higgins et al., 2018). The former factor keeps the newly deposited shallow sediments at or near the seafloor for prolonged periods of time, while the latter one maintains sufficient fluid-sediment exchange reaction. Theoretically, they maintain a good chemical and isotopic equilibrium reaction between the fluid and precipitated minerals. Therefore, when minerals formed under the same extent of fluid-buffered diagenetic conditions, we can consider the isotope fractionation coefficient between minerals and the fluid is constant.

The style (fluid-buffered vs. sediment-buffered) and extent of early marine diagenetic alteration can be identified by isotopic geochemical signals (e.g., $\delta^{13}C$, $\delta^{44/40}Ca$, $\delta^{26}Mg$; (Ahm et al., 2019; Fantle et al., 2020; Fantle & Higgins, 2014; Higgins et al., 2018). However, they are difficult to be identified by either petrographic (Melim et al., 2002) or traditional elemental proxies (e.g., Mn/Sr; Brand & Veizer, 1980). The changes of isotopic compositions during early marine diagenetic alteration mainly depend on two variables, namely (1) abundance of elements in seawater-derived pore-fluids compared to precipitated carbonate minerals, and (2) fluid flowing mechanism (diffusive vs. advective). As major constituents, Mg, Ca, and C abundances in dolomite relative to normal seawater gradually increase, indicating that the resistance of their isotopic compositions to diagenetic alteration progressively increases. Due to the difference in resistance to diagenetic alteration between Mg, Ca, and C isotopes, these isotopes can be used together to quantify the extent of diagenesis. Dominant fluid flowing mechanism driven by various hydrological and geological processes is perhaps the second most important variation in

influencing the diagenetic process. Because it significantly determines the extent to which the diagenetic system for a certain element is fluid-buffered or sediment-buffered. Generally, the diffusive transport creates a sediment-buffered diagenetic environment, whereas the advective fluid flow forms a fluid-buffered condition. In addition, the sedimentation rate greatly dominates the extent of carbonate diagenesis as it controls the length of the chemical reaction and thus determines diffusive or advective reaction length scales.

XK-1 dolomites slowly precipitated via same degree recrystallization under long-term seawater-derived fluid-buffered diagenetic conditions. Dolomite precipitated near the seawater-sediment interface has a fluid-buffered composition with respect to Mg and Ca (Blättler et al., 2015). The Xisha carbonate platform has been surrounded by seawater as it has developed on an isolated uplifted basement far away from the continent since the Neogene. This creates an inherently consistent seawater environment for the formation of the Xisha platform carbonates. The core XK-1 is more susceptible to seawater circulation as it is on the edge of the Xisha platform. For the dolomite intervals of core XK-1, the depositional accumulation rates (DARs) are very low, generally lower than 40 m/Ma, and the depositional hiatus (exposure surface as a sign) occurs frequently (Fig. 2). The low DARs and prolonged depositional hiatuses could keep the unlithified sediments near sea level for a long time, maintain sufficient fluid-sediment chemical exchange reaction, and further transform the precipitated metastable precursor carbonate minerals into more stable dolomites. These conditions including slow sedimentation rates, good seawater circulation, and prolonged depositional hiatuses are all in favor of forming a seawater-influenced fluid-buffered diagenetic environment during XK-1 dolomite formation. Also, Cross-plots of Sr/Ca, $\delta^{13}C$, $\delta^{18}O$, and $\delta^{26}Mg$ vs. $\delta^{44/40}Ca$ values for XK-1 dolomites indicate fluid-buffered diagenetic conditions (Fig. 4). Most significantly, our paired Ca and Mg isotope data strongly support this inference. The $\delta^{26}Mg$ values of XK-1 dolomites range from -2.98 to -2.71‰, with an average value of -2.85‰, which are relatively uniform and around 2‰ lower than that of seawater (-0.83±0.09‰, Ling et al., 2011) (Fig. 4). The $\delta^{44/40}Ca$ values of XK-1 dolomites (1.08~1.35‰), are higher than that of most Monterey Fm. dolomites (0.68~1.08‰, Higgins et al., 2018), which formed under sediment-buffered conditions. Monterey Fm. dolomites are associated with high and variable $\delta^{26}Mg$ values due to distillation of pore-fluid Mg^{2+} and low $\delta^{44/40}Ca$ values inherited from the precursor carbonate. As discussed in detail in Higgins et al. (2018), dolomites precipitated in seawater-similar fluid-buffered conditions are estimated to have relatively homogeneous and low $\delta^{26}Mg$ values that are 2‰ lower than that of seawater, and variable and high $\delta^{44/40}Ca$ values that are approaching to that of seawater. Thus, paired Ca and Mg isotope evidence favors that XK-1 dolomites precipitated under seawater-like fluid-buffered diagenetic conditions with respect to Mg and Ca. In addition, the seawater-similar rare earth element (REE) patterns of all dolomite samples also imply a dolomitizing fluid chemically similar to seawater (Bi et al., 2019). The chemical composition of fluid inclusions hosted in XK-1 dolomites further suggests that the dolomitizing fluids have similar chemical features to high-salinity concentrated normal seawater and the dolomitization should occur in a near-surface environment (Bi et al., 2018a). A seepage-reflux dolomitization model was proposed as a possible explanation for the origin of dolomite in the Xisha Islands (Bi et al., 2018a; Cao et al., 2016). Nevertheless, the timing of dolomitization is critical for us to understand the dolomitization process. The consistency of Sr isotopic compositions ($^{87}Sr/^{86}Sr$ ratios) of Xisha dolomites with that of contemporaneous seawater (Bi et al., 2018b; Fan et al., 2019) indicate these thick successions of dolomite developed through multiple phases of dolomitization.

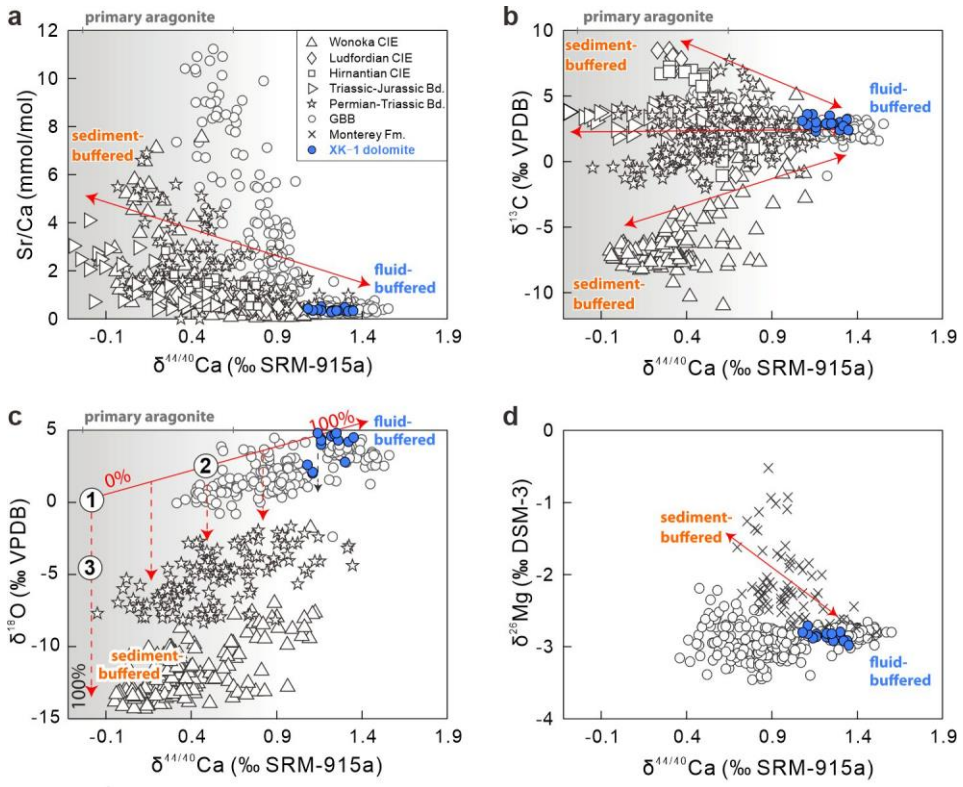

Fig. 4 Cross plots of (a) $\delta^{44/40}Ca$ values versus Sr/Ca ratios, (b) $\delta^{44/40}Ca$ versus $\delta^{13}C$ values, (c) $\delta^{44/40}Ca$ versus $\delta^{18}O$ values and (d) $\delta^{44/40}Ca$ versus $\delta^{26}Mg$ values. All our XK-1 dolomites are plotted together with the ancient and modern carbonate data compiled in Ahm et al. (2018) and Higgins et al. (2018).

In summary, the dolomitization of the XK-1 core carbonates occurred in a diagenetic environment that was seawater-like fluid-buffered with respect to Ca. The chemical information of pure diagenetically precipitated dolomites was completely overprinted by contemporaneous seawater. Therefore, pure dolomites fully recorded the chemical composition of primary paleo-seawater.

5.1.2 Ca isotope fractionation during marine dolomitization and inferred Neogene $\delta^{44/40}Ca_{sw}$

As there is Ca isotopic fractionation between diagenetic precipitated dolomite and seawater, the question remains is whether the fractionation reached an isotopic equilibrium state, in other words, whether the Ca isotope fractionation is equilibrium fractionation. As summarized in the introduction section, the main parameters that control the Ca isotope fractionation of dolomites are mineralogy, mineral precipitation rate, saturation state, and stoichiometry. The dolomite samples studied here are all pure dolomites, of which the dolomite contents are mostly up to 100%, no lower than 95%. Therefore, there is no difference in mineralogical composition, and the degree of Ca isotopic fractionation caused by the mineralogical factor should be identical for all XK-1 dolomite samples. Given that the DARs of XK-1 dolomite intervals are mainly lower than 40 m/Ma and consistent, the mineral precipitation rate will not cause a different degree of Ca isotope fractionation. Similarly, since XK-1 dolomites have continuously precipitated from coeval seawater at an almost uniform rate, the seawater could be regarded as

supersaturated to the same extents with respect to dolomite. So, the similar degree of saturation state is unlikely to result in differential fractionation of Ca isotopes. In dolomite stoichiometry, Ca/(Ca+Mg) molar ratio is an effective stoichiometric index. Lack of correlation between $\delta^{44/40}$Ca values and Ca/(Ca+Mg) molar ratios in XK-1 dolomites indicates that the effect of dolomite stoichiometry on Ca isotope fractionation in this study is negligible (Fig. 5A). In addition, the degree of cation ordering in dolomite is another influencing factor need to be considered for discussing the Ca isotope fractionation in dolomite. Experimental studies have shown that well-ordered dolomite is transformed from metastable disordered proto-dolomite through recrystallization (Kaczmarek & Sibley, 2014). This transformation is common during early stage dolomitization (Kaczmarek & Thornton, 2017), of which the isotopic effects are unknown. The parameter I (015/110), relative intensity of super-lattice X-ray reflection, is a degree indicator of dolomite cation ordering (Goldsmith & Graf, 1958). As there is no correlation between $\delta^{44/40}$Ca values and I (015/110) ratios for XK-1 dolomites, the effect of the cation ordering on the Ca isotope fractionation should be limited (Fig. 5B). In summary, there is no fractionation difference of Ca isotopes between pure XK-1 dolomites, resulting from same degrees of diagenetic alteration during the early dolomitization.

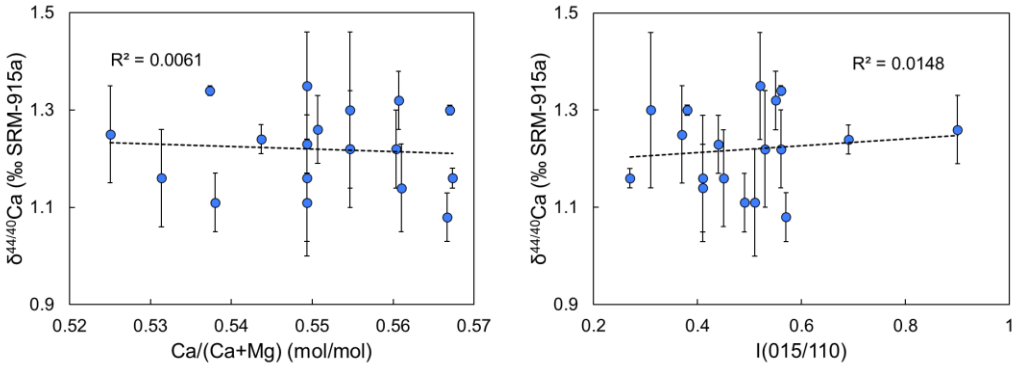

Fig. 5 Cross plots of $\delta^{44/40}$Ca versus Ca/(Ca+Mg) molar ratios (left) and I (015/110) values (right) for XK-1 dolomites. Ca/(Ca+Mg) molar ratio is a stoichiometric index. I (015/110) is a degree indicator of dolomite cation ordering.

The impact of post-depositional diagenetic alteration on the Ca isotope fractionation needs to be considered. We propose such impact should be limited because Ca in dolomite is robust to diagenetic alteration. The resistance of elements in carbonate minerals to diagenetic alteration after burial is mainly determined by the abundance of elements in minerals relative to their ambient pore-fluids (Ahm et al., 2018). The relative abundance ratios of Mg, Ca, and C in XK-1 dolomites in comparison to normal seawater are around 90, 600, and 4 600 respectively, showing a gradually increasing trend of resistance to burial diagenesis. Considering the possibility that C isotopes signals may be affected by remineralization of organic C, Ca becomes the most robust primary isotopic signal recorder in dolomite against post-depositional processes. Furthermore, similar to Mg, high thermodynamic stability of Ca in dolomite makes Ca isotopes less prone to post-depositional resetting (Hu et al., 2017). Therefore, Ca isotopes in XK-1 dolomites are robust to post-depositional diagenetic alteration. In summary, XK-1 dolomites could retain the primary Ca isotopic signals of seawater-similar fluids.

Over the past two decades, many investigations have attempted to reconstruct past changes in $\delta^{44/40}Ca_{sw}$ for the Neogene. Despite of these efforts, there is no definitive Neogene $\delta^{44/40}Ca_{sw}$ record so far because the Neogene records display large differences between various proxy archives, such as bulk carbonate sediments, foraminifera, barites, phosphates, and corals

(Arning et al., 2009; De La Rocha & DePaolo, 2000; Fantle & DePaolo, 2005, 2007; Gothmann et al., 2016; Griffith et al., 2008; Heuser et al., 2005; Schmitt et al., 2003; Sime et al., 2007). These discrepancies between $\delta^{44/40}Ca_{sw}$ records based on different archives have been suggested to be caused by changes in the fractionation factor or a result of diagenesis (Fantle & Tipper, 2014; Gussone et al., 2020; Tipper et al., 2016). Regardless, it is feasible to use multiple tracers to reconstruct $\delta^{44/40}Ca_{sw}$, if the correlation between the fractionation factors of these tracers can be determined (Fantle & Tipper, 2014). However, the research on this correlation is still in debate.

In this study, we found XK-1 dolomites, which were formed in seawater-similar fluid-buffered diagenetic environments to the same extent, could record the pristine seawater chemical information. We demonstrated that there is no fractionation difference of Ca isotopes between XK-1 pure dolomite samples during the dolomitization. The Ca isotope fractionation factor between dolomite and seawater ($\Delta^{44/40}Ca_{dol\text{-}sw}$) was inferred to be between -0.5 and -0.8‰ from the $\delta^{44/40}Ca$ difference between XK-1 dolomites and modern seawater. The inferred value is consistent with the observed $\Delta^{44/40}Ca_{dol\text{-}sw}$ value of -0.4 to -0.7‰ for primary dolomites from two cold seeps near the sea floor in the South China Sea (Wang et al., 2012, 2014). Similarly, a $\Delta^{44/40}Ca_{dol\text{-}fluid}$ value of −0.5 to −0.7 ‰ between primary dolomites and pore water of siliciclastic sediments at the Peru continental margin was revealed (Gussone & Dietzel, 2016). Actually, some studies in early years have suggested a $\Delta^{44/40}Ca$ value of ~0‰ for dolomite recrystallization (Holmden, 2009; Jacobson & Holmden, 2008). They also illustrate that the enrichment or depletion of ^{44}Ca in dolomite relative to the surrounding pore water directly reflects different $\delta^{44/40}Ca$ values of the involved reacting fluid. Blättler et al. (2015) elucidated that the $\delta^{44/40}Ca$ value of dolomite in different depths depends on the Ca isotopic composition of pore water, assuming a constant $\Delta^{44/40}Ca_{dol\text{-}fluid}$. To conclude, these studies support our findings that XK-1 dolomites record the primary $\delta^{44/40}Ca_{sw}$ for the Neogene.

5.2 A simple Ca isotope mass balance box model and its implications for carbonate burial and climate change

5.2.1 Modeling the Neogene Ca cycle

The weathering of Ca from silicates and its final sequestration in marine carbonates plays an important role in controlling the concentration of CO_2 in the atmosphere (Berner et al., 1983; Raymo & Ruddiman, 1992). The concentration of Ca ion in the ocean has varied over the Phanerozoic time (Hardie, 1996; Holland, 1984). During the Cenozoic, it decreased from ~22 to 10 mmol/kg (modern value), which were recorded in fluid inclusions of evaporites (Brennan et al., 2013; Horita et al., 2002; Lowenstein et al., 2003). Fundamentally, the Ca concentration of seawater is governed by the relative proportion of the Ca input to and Ca output out of the ocean. When the inputs and outputs are in balance, the ocean will be at steady state with respect to Ca. In the modern ocean, the concentration and isotope ratio of Ca are both considered homogeneous (Zhu & Macdougall, 1998). Therefore, the modern ocean is believed to be at steady state with respect to Ca. The main Ca fluxes of the inputs and outputs to and out of the modern ocean and their $\delta^{44/40}Ca$ values are listed in Table 2.

Table 2. Simplified modern ocean Ca budget. The main fluxes and isotopic compositions of the Ca inputs and outputs indicate a steady state for the modern ocean

Inputs	**Flux ($Tmol\ yr^{-1}$)**	**References**	**$\delta^{44/40}Ca$ (‰)**	**References**
Riverine	13.2	Milliman (1993) Milliman & Droxler (1996)	0.86	Heuser et al. (2005) Schmitt et al. (2003) Tipper et al. (2006) Zhu & Macdougall (1998)
Submarine groundwater discharge	16	Holmden et al. (2012)	0.65	Holmden et al. (2012)
High-T hydrothermal	2.8	Amini et al. (2006) Amini et al. (2008) Schmitt et al. (2003)	0.93	Amini et al. (2008)
Total input	**32**		**0.76**	
Outputs				
Holocene carbonates	**32**	Milliman (1993) Milliman & Droxler (1996)	**0.76**	Fantle & Tipper (2014) Holmden et al. (2012) Tipper et al. (2016)

The Ca isotope mass balance model for the Neogene ocean was established based on two main assumptions. First, the Ca cycle in the Neogene ocean was close to steady state, which is similar to the modern Ca cycle. For the modern ocean, the large Ca inventory and relatively small input (or output) flux yield a long residence time for Ca (~1 Ma). Due to its significantly longer residence time than the ocean mixing time (~1 kyr) (Hippler et al., 2003), Ca is homogeneous with respect to both its concentrations and isotopic ratios throughout the ocean (Zhu & Macdougall, 1998). The similarity in both the Ca fluxes of the major marine inputs and outputs and their Ca isotopic compositions (DePaolo, 2004; Wallmann, 2001) indicates that the modern ocean is at steady state with respect to Ca (Berner, 2004; De La Rocha & DePaolo, 2000; Hardie, 1996; Schmitt et al., 2003; Skulan et al., 1997). Recent work has shown that this is probably true as well over geologic time scales (Blättler & Higgins, 2017), so this should also be the case for the Neogene. Second, the Ca isotopic compositions from the Ca inputs into the Neogene ocean were the same as those of the modern marine inputs. The main sources of Ca to the ocean are rivers, submarine groundwater discharge and hydrothermal fluids (Griffith et al., 2020; Holmden et al., 2012; Tipper et al., 2016). Given no considerable difference between $\delta^{44/40}Ca$ values of these sources (Fantle & Tipper, 2014; Holmden et al., 2012; Schmitt et al., 2003), the average Ca isotopic composition of global inputs should be constant over time.

Consequently, non-steady state is likely to be caused by changes in input and output Ca fluxes rather than changes in Ca isotopic compositions (Schmitt et al., 2003). The major Ca sink from the ocean is carbonate precipitation. Since the emergence and accumulation of pelagic limestone in the late Mesozoic (Wilkinson & Walker, 1989), shallow-water carbonates and pelagic carbonates have become the two main sinks of Ca in the ocean. Both of them fractionate lighter Ca relative to seawater when they precipitate from seawater (De La Rocha & DePaolo, 2000; DePaolo, 2004; Gussone & Heuser, 2016; Skulan et al., 1997). As described by DePaolo (2004), Fantle (2010) and Fantle and Tipper (2014), the $\delta^{44/40}Ca_{sw}$ value through time is mainly controlled by the Ca isotope fractionation between seawater and average carbonate ($\Delta^{44/40}{}_{carb}$). $\Delta^{44/40}{}_{carb}$ is determined not only by the fractionation factor between each sink and seawater, but also by the relative mass of Ca removed by each sink ($\Delta^{44/40}{}_{carb}=(F_{shallow}\Delta^{44/40}{}_{shallow}+F_{pelagic}\Delta^{44/40}{}_{pelagic})/(F_{shallow}+F_{pelagic})$. Therefore, we propose a Ca isotope mass balance box model to explore the Ca output proportions between shallow-water carbonates and pelagic carbonates (Fig. 6).

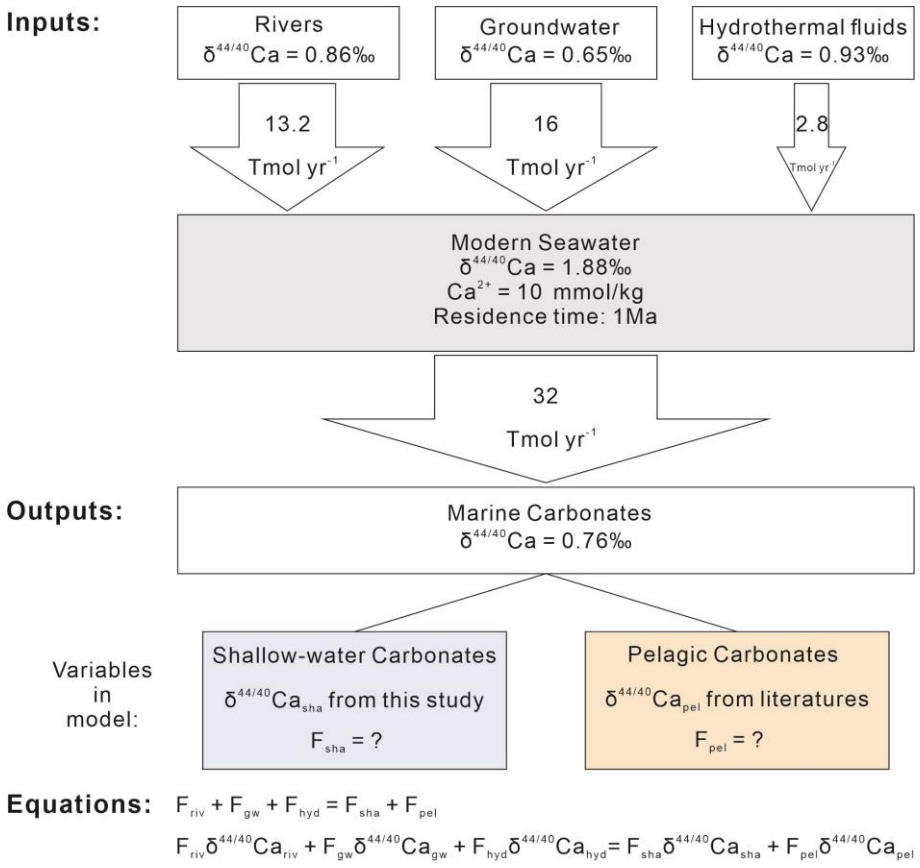

Fig. 6 Box model of the Ca isotope fluxes into and out of the ocean. In the equations, F_{riv}, F_{gw} and F_{hyd} represent the riverine, groundwater, and hydrothermal input flux of Ca to the ocean; F_{sha} and F_{pel} refer to the Ca output flux of shallow-water carbonates and pelagic carbonates from the ocean, respectively. The $\delta^{44/40}Ca$ values for Ca fluxes F_{riv}, F_{gw}, F_{hyd}, F_{sha}, and F_{pel} are denoted as $\delta^{44/40}Ca_{riv}$, $\delta^{44/40}Ca_{gw}$, $\delta^{44/40}Ca_{hyd}$, $\delta^{44/40}Ca_{sha}$, and $\delta^{44/40}Ca_{pel}$. For the inputs, the Ca flux estimates (F_{riv}, F_{gw}, F_{hyd}) are from the literature (Amini et al., 2006; Amini et al., 2008; Milliman, 1993; Milliman and Droxler, 1996; Holmden et al., 2012; Schmitt et al., 2003) and their isotopic compositions ($\delta^{44/40}Ca_{riv}$, $\delta^{44/40}Ca_{gw}$, $\delta^{44/40}Ca_{hyd}$) are from the literature (Amini et al., 2008;

Heuser et al., 2005; Holmden et al., 2012; Schmitt et al., 2003; Tipper et al., 2006; Zhu and Macdougall, 1998). For the outputs, the Ca flux estimate of average bulk carbonates (F_{carb}) is from the literature (Milliman, 1993; Milliman and Droxler, 1996) and its Ca isotopic composition ($\delta^{44/40}Ca_{carb}$) is from the literature (Fantle and Tipper, 2014; Holmden et al., 2012; Tipper et al., 2016), the Ca isotopic composition of shallow-water carbonates ($\delta^{44/40}Ca_{sha}$) is from this study, and the Ca isotopic composition of pelagic carbonates ($\delta^{44/40}Ca_{pel}$) is from the literature (De La Rocha and DePaolo, 2000; Fantle and DePaolo, 2005, 2007; Fantle and Higgins, 2014). Therefore, F_{sha} and F_{pel} are two unknowns to be determined.

Assuming Neogene seawater stays at steady state with respect to Ca, then we have

$$F_{input} = F_{output} \quad (1)$$

$$\delta^{44/40}Ca_{sw} = \delta^{44/40}Ca_{input} - \Delta^{44/40}{}_{carb} \quad (2)$$

where F_{input} and F_{output} refer to the mass flux of Ca into and out of the ocean, $\delta^{44/40}Ca_{sw}$ is the Ca isotopic composition of seawater, $\delta^{44/40}Ca_{input}$ is the flux-weighted average Ca isotopic composition of the inputs to the ocean, $\Delta^{44/40}{}_{carb}$ is the flux-weighted average Ca isotopic composition of the outputs relative to seawater.

Therefore, we can write the equations (1) and (2) as:

$$F_{riv} + F_{gw} + F_{hyd} = F_{sha} + F_{pel} \quad (3)$$

$$F_{riv}\delta^{44/40}Ca_{riv} + F_{gw}\delta^{44/40}Ca_{gw} + F_{hyd}\delta^{44/40}Ca_{hyd} = F_{sha}\delta^{44/40}Ca_{sha} + F_{pel}\delta^{44/40}Ca_{pel} \quad (4)$$

where F_{riv}, F_{gw} and F_{hyd} represent the riverine, groundwater, and hydrothermal input flux of Ca to the ocean; F_{sha} and F_{pel} refer to the Ca output flux of shallow-water carbonates and pelagic carbonates from the ocean, respectively. The $\delta^{44/40}Ca$ values for Ca fluxes F_{riv}, F_{gw}, F_{hyd}, F_{sha}, and F_{pel} are denoted as $\delta^{44/40}Ca_{riv}$, $\delta^{44/40}Ca_{gw}$, $\delta^{44/40}Ca_{hyd}$, $\delta^{44/40}Ca_{sha}$, and $\delta^{44/40}Ca_{pel}$.

We select only carbonate layers with approximately 100% dolomite content or 100% calcite content for calculation and discussion to accurately constrain the Ca output fluxes and their isotopic compositions in shallow-water carbonates. For time intervals when pure dolomite forms, we have

$$\delta^{44/40}Ca_{sha} = \delta^{44/40}Ca_{dol} \quad (5)$$

For time intervals when pure calcite forms, we do not use the $\delta^{44/40}Ca$ values in the calcite samples. As we explained in section 5.1, pure dolomite could record primary seawater chemistry whereas calcite was probably not pristine because of the ambiguous influence of various biominerals. However, we could use an empirical formula to calculate the $\delta^{44/40}Ca_{cal}$ value here.

$$\delta^{44/40}Ca_{sha} = \delta^{44/40}Ca_{cal} = \delta^{44/40}Ca_{dol} - 0.3 \quad (6)$$

Here the value 0.3 is the difference in the mean Ca isotopic compositions between calcite and dolomite (Artemov et al., 1967; Böhm et al., 2005; Heuser et al., 2005).

Put parameters in equations (5) or (6) into equations (3) and (4). Then for equations (3) and (4), we have four unknowns, namely $\delta^{44/40}Ca_{dol}$, $\delta^{44/40}Ca_{pel}$, F_{sha}, and F_{pel}. The Ca isotopic composition of dolomites ($\delta^{44/40}Ca_{dol}$) can be obtained from this study, whereas the Ca isotopic composition of pelagic carbonates ($\delta^{44/40}Ca_{pel}$) is compiled from the literature (De La Rocha &

DePaolo, 2000; Fantle & DePaolo, 2005, 2007; Fantle & Higgins, 2014) (Fig. 7). At last, two unknowns are left for equations (3) and (4), namely F_{sha} and F_{pel}. Therefore, we can quantify the fluxes of F_{sha} and F_{pel}, that is, the relative fluxes of shallow-water carbonates and pelagic carbonates during the Neogene period (Fig. 8).

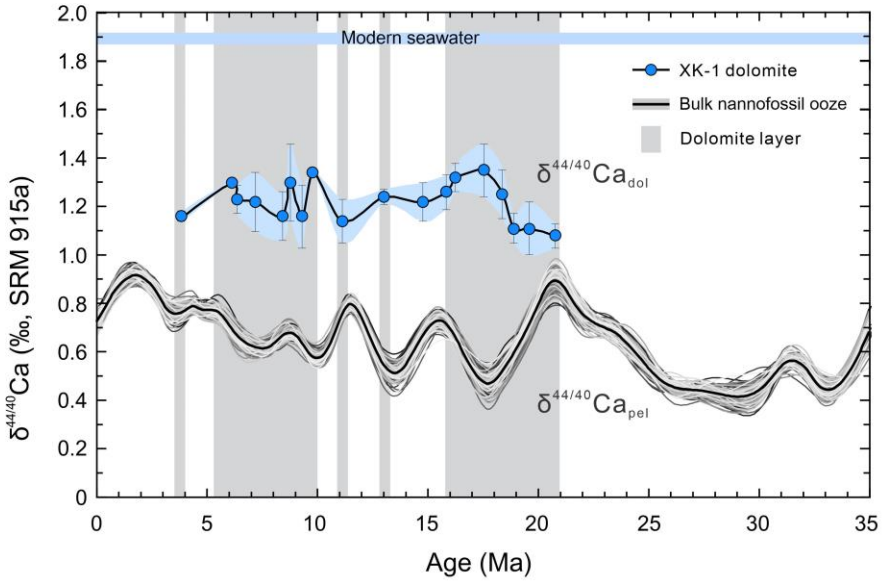

Fig. 7 The Ca output fluxes of shallow-water carbonates and pelagic carbonates during the Neogene. The Ca isotopic composition of dolomites ($\delta^{44/40}Ca_{dol}$) is from this study, whereas the Ca isotopic composition of pelagic carbonates ($\delta^{44/40}Ca_{pel}$) can be obtained from the literature (De La Rocha & DePaolo, 2000; Fantle & DePaolo, 2005, 2007; Fantle & Higgins, 2014;).

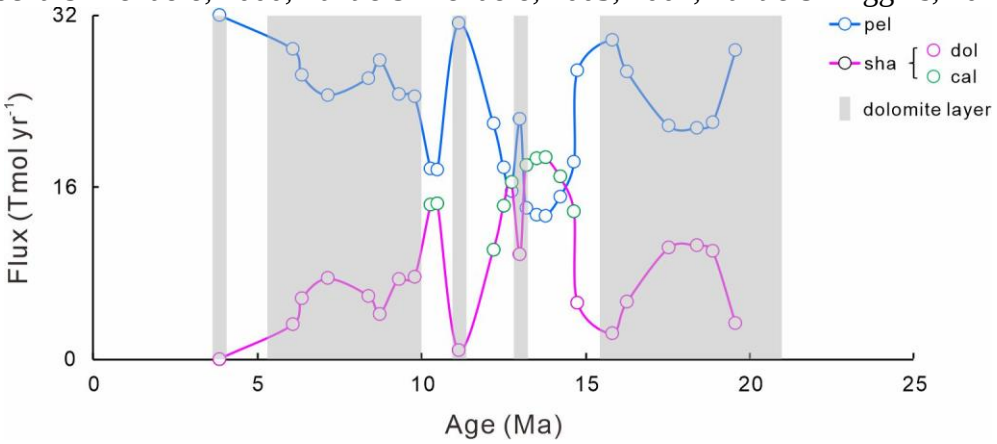

Fig. 8 The Ca output fluxes out of the ocean caused by shallow-water carbonate burial and pelagic carbonate burial during the Neogene. Note: "pel" denotes pelagic carbonate burial, "sha" denotes shallow-water carbonate burial, "dol" denotes dolomites, "cal" denotes calcites. Dolomite layer corresponds to when XK-1 massive dolomites formed. The Modeling data can be found in the supporting information.

Our model result shows that the Ca output flux from the ocean of shallow-water carbonates is mirrored by that of pelagic carbonates at steady state during the Neogene (Fig. 8). Strikingly, in the time intervals when the dolomite form, pelagic carbonate burial dominate the marine Ca output flux. Hence, the pelagic carbonate burial must be related to the formation of marine dolomite.

5.2.2 Relationship between marine carbonate burial, continental weathering, seawater chemistry, and climate change

Throughout the Neogene, continental silicate weathering increased, which has been suggested by previous studies of seawater Sr isotopes (McArthur et al., 2012) and Li isotopes (Misra & Froelich, 2012; Wanner et al., 2014). The Mg and Ca ions can be brought to the ocean in large quantities through silicate weathering via riverine delivery. However, the Ca ion concentration in seawater has been decreasing during the Neogene although the Mg ion concentration has been increasing. The increase of seawater Mg^{2+} indicates that the Mg input flux to the ocean (weathering flux) exceeds the Mg output flux out of the ocean (hydrothermal flux and sedimentary flux). But what processes led to the decreasing of seawater Ca^{2+} concentration? Both weathering and hydrothermal processes contribute Ca^{2+} to the ocean. It is known that Ca^{2+} in seawater must have been removed by its major sink (carbonate burial, either in shallow-water or pelagic carbonates). The formation of massive dolomites in Xisha area corresponds to the rapid increase in both seawater $^{87}Sr/^{86}Sr$ ratios (Bi et al., 2018b; Fan et al., 2019; McArthur et al., 2012) and seawater Li isotopic compositions (Misra & Froelich, 2012), which probably indicate enhanced continental silicate weathering. During the rapidly enhanced weathering periods, significant quantities of Ca^{2+} were delivered to seawater. Also, along with the formation of massive dolomites, amounts of Ca^{2+} were released to seawater by substituting Mg^{2+} in dolomite. Where did the reduced Ca^{2+} in the ocean go? As our model predicts, the disappeared Ca^{2+} fell into the deep sea and was sequestered by pelagic carbonates. The observed increase of $\delta^{44/40}Ca_{sw}$ based on our dolomite record could also be explained by more pelagic carbonate burial through preferential removal of isotopically light Ca from seawater. We have elucidated in Section 5.1 that the Xisha dolomite was formed in a seawater-buffered diagenetic environment near the seawater-sediment interface. The uplift of the Qinghai-Tibet Plateau led to the subsidence of the Xisha platform (Wu et al., 2014) and enhanced continental weathering. Enhanced weathering will consume more atmospheric CO_2, causing global cooling and subsequent sea-level fall. These superimposed factors created a near seawater-sediment interface environment in favor of dolomite formation. At the same time, a large amount of weathering products (dissolved calcium and carbon) was eventually buried in pelagic carbonates. In addition, due to the sea level decline, some shallow shelf carbonates were exposed to the atmosphere, weathered, and then transported to the deep sea, which is called carbonate accumulation shifting (Milliman & Droxler, 1996). Our findings are consistent with those of van der Ploeg et al. (2019), which suggested that enhanced continental weathering may have driven a simultaneous increase in pelagic carbonate burial. In their study, they used a global carbonate alkalinity mass balance model to define the Cenozoic alkalinity removal fluxes due to marginal (shallow-water) carbonate burial or pelagic carbonate burial. In addition, recent studies suggested that during the glacial period, more CO_2 was sequestered in intermediate waters of the deep ocean (Chen et al., 2020; Yu et al., 2020). Because it is easy to reach CO_2 dynamic balance between the shallow sea and the atmosphere, the shallow sea will not store much CO_2 for a long time. Therefore, during the glacial period, extra CO_2 may have been sequestered into deep sea, which was in turn buried by pelagic carbonates in the long-term time scales. As a result, the seawater Ca^{2+} concentration has decreased over the Neogene. Our work reinforces the role of pelagic carbonate accumulation in impacting the global carbon cycle and seawater chemistry.

5 Conclusions

In this study, we report the Ca isotopic compositions ($\delta^{44/40}Ca$) of pure dolomites in the core XK-1 from the Xisha Islands in the South China Sea. We suggest that XK-1 dolomites probably formed in seawater-like fluid-buffered diagenetic environments near the seawater-sediment interface. Moreover, no Ca isotope fractionation between XK-1 dolomites and seawater was observed. Therefore, we conclude that XK-1 dolomites could retain the primary seawater chemistry and record contemporaneous seawater Ca isotopic compositions ($\delta^{44/40}Ca_{sw}$). We infer the Ca isotope fractionation factor between dolomite and seawater ($\Delta^{44/40}Ca_{dol\text{-}sw}$) to be between -0.5 and -0.8‰, consistent with the values reported in previous studies. In addition, we adopt a Ca isotope mass balance box model to quantitatively constrain respective contributions from shallow-water and pelagic carbonates in sequestering carbon during the Neogene. Based on the model results, we explore the long-term relationship between continental weathering, climate change, sea-level fluctuation, seawater chemistry, and carbonate burial. Finally, we conclude that pelagic carbonate burial may have sequestered more carbon than previously estimated during the global cooling period.

Acknowledgments, Samples, and Data

This work was funded by the National Science and Technology Major Project (No. 2011ZX05025-002-03), the Project of China National Offshore Oil Corporation (CNOOC) Limited (No. CCL2013ZJFNO729), and the Overseas Joint Training Project for Doctoral Students of Ocean University of China. We thank Hongli zhu, Fang Liu, and Yongli Xue from the State Key Laboratory of Isotope Geochemistry, Guangzhou Institute of Geochemistry, Chinese Academy of Sciences, for their help in the Ca isotope experiment. All data including measured and modeling data supporting the findings of this study are available within the paper and in the supporting information, where we clearly state the data source.

References

Ahm, A. S. C., Bjerrum, C. J., Blättler, C. L., Swart, P. K., & Higgins, J. A. (2018). Quantifying early marine diagenesis in shallow-water carbonate sediments. *Geochimica et Cosmochimica Acta*, *236*, 140–159. https://doi.org/10.1016/j.gca.2018.02.042

Ahm, A. S. C., Maloof, A. C., Macdonald, F. A., Hoffman, P. F., Bjerrum, C. J., Bold, U., et al. (2019). An early diagenetic deglacial origin for basal Ediacaran "cap dolostones." *Earth and Planetary Science Letters*, *506*, 292–307. https://doi.org/10.1016/j.epsl.2018.10.046

AlKhatib, M., & Eisenhauer, A. (2017). Calcium and strontium isotope fractionation in aqueous solutions as a function of temperature and reaction rate; I. Calcite. *Geochimica et Cosmochimica Acta*, *209*, 296–319. https://doi.org/10.1016/j.gca.2016.09.035

Arning, E. T., Lückge, A., Breuer, C., Gussone, N., Birgel, D., & Peckmann, J. (2009). Genesis of phosphorite crusts off Peru. *Marine Geology*, *262*(1), 68–81. https://doi.org/https://doi.org/10.1016/j.margeo.2009.03.006

Artemov, Y. M., Strizhov, V. P., Ustinov, V. I., & Yaroshevskiy, A. A. (1967). Possible isotope fractionation during dolomitization. *Geokhimiya*, *5*, 519–529.

Bernard, S., Daval, D., Ackerer, P., Pont, S., & Meibom, A. (2017). Burial-induced oxygen-isotope re-equilibration of fossil foraminifera explains ocean paleotemperature paradoxes. *Nature Communications*, *8*(1), 1134. https://doi.org/10.1038/s41467-017-01225-9

Berner, R. A., Lasaga, A. C., & Garrels, R. M. (1983). The carbonate-silicate geochemical cycle and its effect on atmospheric carbon dioxide over the past 100 million years. *American Journal of Science*. https://doi.org/10.2475/ajs.283.7.641

Berner, Robert A. (2004). A model for calcium, magnesium and sulfate in seawater over Phanerozoic time. *American Journal of Science*, *304*(5), 438–453. https://doi.org/10.2475/ajs.304.5.438

Berner, Robert A, & Berner, E. K. (1997). Silicate Weathering and Climate BT - Tectonic Uplift and Climate Change. In W. F. Ruddiman (Ed.) (pp. 353–365). Boston, MA: Springer US. https://doi.org/10.1007/978-1-4615-5935-1_15

Bi, D. (2019). *Geochemical characters of reef carbonates from the Xisha Islands (South China Sea) and its implications for paleoenvironments*. Ocean University of China.

Bi, D., Zhai, S., Zhang, D., Liu, X., Liu, X., Jiang, L., & Zhang, A. (2018). Constraints of fluid inclusions and C, O isotopic compositions on the origin of the dolomites in the Xisha Islands, South China Sea. *Chemical Geology*, *493*, 504–517. https://doi.org/https://doi.org/10.1016/j.chemgeo.2018.07.005

Bi, D., Zhang, D., Zhai, S., Liu, X. X., Xiu, C., Liu, X. X., et al. (2018). Seawater 87Sr/86 Sr values recorded by reef carbonates from the Xisha Islands (South China Sea) since the Neogene and its response to the uplift of Qinghai-Tibetan Plateau. *Geological Journal*, (October), 1–13. https://doi.org/10.1002/gj.3386

Bi, D., Zhai, S., Zhang, D., Xiu, C., Liu, X. X., Liu, X. X., et al. (2019). Geochemical Characteristics of the Trace and Rare Earth Elements in Reef Carbonates from the Xisha Islands (South China Sea): Implications for Sediment Provenance and Paleoenvironment. *Journal of Ocean University of China*, *18*(6), 1291–1301. https://doi.org/10.1007/s11802-019-3790-0

Blättler, C. L., & Higgins, J. A. (2017). Testing Urey's carbonate–silicate cycle using the calcium isotopic composition of sedimentary carbonates. *Earth and Planetary Science Letters*, *479*, 241–251. https://doi.org/10.1016/j.epsl.2017.09.033

Blättler, C. L., Miller, N. R., & Higgins, J. A. (2015). Mg and Ca isotope signatures of authigenic dolomite in siliceous deep-sea sediments. *Earth and Planetary Science Letters*, *419*, 32–42. https://doi.org/10.1016/j.epsl.2015.03.006

Böhm, F., Eisenhauer, A., Heuser, A., & Kiessling, W. (2005). Calcium Isotope Fractionation During Dolomitization.

Brand, U., & Veizer, J. (1980). Chemical diagenesis of a multicomponent carbonate system; 1, Trace elements. *Journal of Sedimentary Research*, *50*(4), 1219–1236. https://doi.org/10.1306/212F7BB7-2B24-11D7-8648000102C1865D

Brennan, S. T., Lowenstein, T. K., & Cendon, D. I. (2013). The major-ion composition of cenozoic seawater: the past 36 million years from fluid inclusions inmarine halite. *American Journal of Science*, *313*(8), 713–775. https://doi.org/10.2475/08.2013.01

Budd, D. A. (1997). Cenozoic dolomites of carbonate islands: their attributes and origin. *Earth-Science Reviews*, *42*(1), 1–47. https://doi.org/https://doi.org/10.1016/S0012-8252(96)00051-7

Cao, J., Zhang, D., Zhai, S., Luo, W., Xiu, C., Liu, X., et al. (2016). The characteristics and genetic model of the dolomitization in Xisha Reef Islands. *Haiyang Xuebao*, *38*(11), 125–139. https://doi.org/10.3969/j. issn. 0253-4193.2016.11.012

Chanda, P., Gorski, C. A., Oakes, R. L., & Fantle, M. S. (2019). Low temperature stable mineral recrystallization of foraminiferal tests and implications for the fidelity of geochemical

proxies. *Earth and Planetary Science Letters*, *506*, 428–440. https://doi.org/10.1016/j.epsl.2018.11.011

Chang, B., Li, C., Liu, D., Foster, I., Tripati, A., Lloyd, M. K., et al. (2020). Massive formation of early diagenetic dolomite in the Ediacaran ocean: Constraints on the "dolomite problem." *Proceedings of the National Academy of Sciences*, *117*(25), 14005 LP – 14014. https://doi.org/10.1073/pnas.1916673117

Chen, T., Robinson, L. F., Burke, A., Claxton, L., Hain, M. P., Li, T., et al. (2020). Persistently well-ventilated intermediate-depth ocean through the last deglaciation. *Nature Geoscience*, *13*(11), 733–738. https://doi.org/10.1038/s41561-020-0638-6

DePaolo, D. J. (2004). Calcium isotopic variations produced by biological, kinetic, radiogenic and nucleosynthetic processes. *Reviews in Mineralogy and Geochemistry*, *55*, 255–288. https://doi.org/10.2138/gsrmg.55.1.255

DePaolo, D. J. (2011). Surface kinetic model for isotopic and trace element fractionation during precipitation of calcite from aqueous solutions. *Geochimica et Cosmochimica Acta*, *75*(4), 1039–1056. https://doi.org/10.1016/j.gca.2010.11.020

Elderfield, H. (2010). Seawater chemistry and climate. *Science*, *327*(5969), 1092–1093.

Fan, T., Yu, K., Zhao, J., Jiang, W., Xu, S., Zhang, Y., et al. (2019). Strontium isotope stratigraphy and paleomagnetic age constraints on the evolution history of coral reef islands, northern South China Sea. *GSA Bulletin*, (X), 1–14. https://doi.org/10.1130/b35088.1

Fantle, M. S., & DePaolo, D. J. (2005). Variations in the marine Ca cycle over the past 20 million years. *Earth and Planetary Science Letters*, *237*(1–2), 102–117. https://doi.org/10.1016/j.epsl.2005.06.024

Fantle, M. S., & DePaolo, D. J. (2007). Ca isotopes in carbonate sediment and pore fluid from ODP Site 807A: The Ca2+(aq)-calcite equilibrium fractionation factor and calcite recrystallization rates in Pleistocene sediments. *Geochimica et Cosmochimica Acta*, *71*(10), 2524–2546. https://doi.org/10.1016/j.gca.2007.03.006

Fantle, M. S., & Higgins, J. (2014). The effects of diagenesis and dolomitization on Ca and Mg isotopes in marine platform carbonates: Implications for the geochemical cycles of Ca and Mg. *Geochimica et Cosmochimica Acta*, *142*, 458–481. https://doi.org/10.1016/j.gca.2014.07.025

Fantle, M. S., & Tipper, E. T. (2014). Calcium isotopes in the global biogeochemical Ca cycle: Implications for development of a Ca isotope proxy. *Earth-Science Reviews*, *129*, 148–177. https://doi.org/10.1016/j.earscirev.2013.10.004

Fantle, M. S., Barnes, B. D., & Lau, K. V. (2020). The Role of Diagenesis in Shaping the Geochemistry of the Marine Carbonate Record. *Annual Review of Earth and Planetary Sciences*, *48*(1), 549–583. https://doi.org/10.1146/annurev-earth-073019-060021

Farkaš, J. (2018). Calcium Isotopes BT - Encyclopedia of Geochemistry: A Comprehensive Reference Source on the Chemistry of the Earth. In W. M. White (Ed.) (pp. 181–186). Cham: Springer International Publishing. https://doi.org/10.1007/978-3-319-39312-4_237

Fouke, B. W., Beets, C. J., Meyers, W. J., Hanson, G. N., & Melillo, A. J. (1996). 87Sr/86Sr Chronostratigraphy and dolomitization history of the Seroe Domi Formation, Curaçao (Netherlands Antilles). *Facies*, *35*(1), 293–320. https://doi.org/10.1007/BF02536966

Goldsmith, J. R., & Graf, D. L. (1958). Structural and Compositional Variations in Some Natural Dolomites. *The Journal of Geology*, *66*(6), 678–693. Retrieved from http://www.jstor.org/stable/30056855

Gothmann, A. M., Bender, M. L., Blättler, C. L., Swart, P. K., Giri, S. J., Adkins, J. F., et al. (2016). Calcium isotopes in scleractinian fossil corals since the Mesozoic: Implications for vital effects and biomineralization through time. *Earth and Planetary Science Letters*, *444*, 205–214. https://doi.org/10.1016/j.epsl.2016.03.012

Griffith, E. M., & Fantle, M. S. (2020). Introduction to calcium isotope geochemistry: Past lessons and future directions. *Chemical Geology*, *537*, 119470. https://doi.org/10.1016/j.chemgeo.2020.119470

Griffith, E. M., Paytan, A., Caldeira, K., Bullen, T. D., & Thomas, E. (2008). A dynamic marine calcium cycle during the past 28 million years. *Science*, *322*(5908), 1671–1674. https://doi.org/10.1126/science.1163614

Griffith, E. M., Schmitt, A. D., Andrews, M. G., & Fantle, M. S. (2020). Elucidating modern geochemical cycles at local, regional, and global scales using calcium isotopes. *Chemical Geology*, *534*. https://doi.org/10.1016/j.chemgeo.2019.119445

Gussone, N., & Dietzel, M. (2016). Calcium Isotope Fractionation During Mineral Precipitation from Aqueous Solution. In *Calcium Stable Isotope Geochemistry* (pp. 75–110). Berlin, Heidelberg: Springer Berlin Heidelberg. https://doi.org/10.1007/978-3-540-68953-9_3

Gussone, N., & Heuser, A. (2016). Biominerals and Biomaterial. In *Calcium Stable Isotope Geochemistry* (pp. 111–144). Berlin, Heidelberg: Springer Berlin Heidelberg. https://doi.org/10.1007/978-3-540-68953-9_4

Gussone, N., Böhm, F., Eisenhauer, A., Dietzel, M., Heuser, A., Teichert, B. M. A., et al. (2005). Calcium isotope fractionation in calcite and aragonite. *Geochimica et Cosmochimica Acta*, *69*(18), 4485–4494. https://doi.org/10.1016/j.gca.2005.06.003

Gussone, N., Langer, G., Thoms, S., Nehrke, G., Eisenhauer, A., Riebesell, U., & Wefer, G. (2006). Cellular calcium pathways and isotope fractionation in Emiliania huxleyi. *Geology*, *34*(8), 625–628. https://doi.org/10.1130/G22733.1

Gussone, N., Ahm, A.-S. C., Lau, K. V, & Bradbury, H. J. (2020). Calcium isotopes in deep time: Potential and limitations. *Chemical Geology*, *544*, 119601. https://doi.org/10.1016/j.chemgeo.2020.119601

Hardie, L. A. (1996). Secular variation in seawater chemistry: An explanation for the coupled secular variation in the mineralogies of marine limestones and potash evaporites over the past 600 m.y. *Geology*, *24*(3), 279. https://doi.org/10.1130/0091-7613(1996)024<0279:SVISCA>2.3.CO;2

Harouaka, K., Eisenhauer, A., & Fantle, M. S. (2014). Experimental investigation of Ca isotopic fractionation during abiotic gypsum precipitation. *Geochimica et Cosmochimica Acta*, *129*, 157–176. https://doi.org/10.1016/j.gca.2013.12.004

He, Q., & Zhang, M. (1986). *Reef Geology of the Xisha Islands, China*. Beijing, China: Science Press. Retrieved from file://catalog.hathitrust.org/Record/102220306

Heuser, A., Eisenhauer, A., Böhm, F., Wallmann, K., Gussone, N., Pearson, P. N., et al. (2005). Calcium isotope (δ44/40Ca) variations of Neogene planktonic foraminifera. *Paleoceanography*, *20*(2), 1–13. https://doi.org/10.1029/2004PA001048

Higgins, J. A., Blättler, C. L., Lundstrom, E. A., Santiago-Ramos, D. P., Akhtar, A. A., Crüger Ahm, A. S., et al. (2018). Mineralogy, early marine diagenesis, and the chemistry of shallow-water carbonate sediments. *Geochimica et Cosmochimica Acta*, *220*, 512–534. https://doi.org/10.1016/j.gca.2017.09.046

Hippler, D., Schmitt, A. D., Gussone, N., Heuser, A., Stille, P., Eisenhauer, A., & Nägler, T. F. (2003). Calcium isotopic composition of various reference materials and seawater.

Geostandards Newsletter, *27*(1), 13–19. https://doi.org/10.1111/j.1751-908X.2003.tb00709.x

Holland, H. D. (1984). *The chemical evolution of the atmosphere and oceans*. Princeton University Press.

Holmden, C, Papanastassiou, D. A., Blanchon, P., & Evans, S. (2012). δ44/40Ca variability in shallow water carbonates and the impact of submarine groundwater discharge on Ca-cycling in marine environments. *Geochimica Et Cosmochimica Acta*, *83*, 179–194. https://doi.org/10.1016/j.gca.2011.12.031

Holmden, Chris. (2009). Ca isotope study of Ordovician dolomite, limestone, and anhydrite in the Williston Basin: Implications for subsurface dolomitization and local Ca cycling. *Chemical Geology*, *268*(3–4), 180–188. https://doi.org/10.1016/j.chemgeo.2009.08.009

Horita, J., Zimmermann, H., & Holland, H. D. (2002). Chemical evolution of seawater during the Phanerozoic: Implications from the record of marine evaporites. *Geochimica et Cosmochimica Acta*, *66*(21), 3733–3756. https://doi.org/10.1016/S0016-7037(01)00884-5

Hu, Z., Hu, W., Wang, X., Lu, Y., Wang, L., Liao, Z., & Li, W. (2017). Resetting of Mg isotopes between calcite and dolomite during burial metamorphism: Outlook of Mg isotopes as geothermometer and seawater proxy. *Geochimica et Cosmochimica Acta*, *208*, 24–40. https://doi.org/10.1016/j.gca.2017.03.026

Husson, J. M., Higgins, J. A., Maloof, A. C., & Schoene, B. (2015). Ca and Mg isotope constraints on the origin of Earth's deepest δ13C excursion. *Geochimica et Cosmochimica Acta*, *160*, 243–266. https://doi.org/10.1016/j.gca.2015.03.012

Inoue, M., Gussone, N., Koga, Y., Iwase, A., Suzuki, A., Sakai, K., & Kawahata, H. (2015). Controlling factors of Ca isotope fractionation in scleractinian corals evaluated by temperature, pH and light controlled culture experiments. *Geochimica et Cosmochimica Acta*, *167*, 80–92. https://doi.org/10.1016/j.gca.2015.06.009

Jacobson, A. D., & Holmden, C. (2008). δ44Ca evolution in a carbonate aquifer and its bearing on the equilibrium isotope fractionation factor for calcite. *Earth and Planetary Science Letters*, *270*(3–4), 349–353. https://doi.org/10.1016/j.epsl.2008.03.039

Jones, B., Luth, R. W., & MacNeil, A. J. (2001). Powder X-Ray Diffraction Analysis of Homogeneous and Heterogeneous Sedimentary Dolostones. *Journal of Sedimentary Research*, *71*(5), 790–799. https://doi.org/10.1306/2DC40968-0E47-11D7-8643000102C1865D

Kaczmarek, S. E., & Sibley, D. F. (2014). Direct physical evidence of dolomite recrystallization. *Sedimentology*, *61*(6), 1862–1882. https://doi.org/https://doi.org/10.1111/sed.12119

Kaczmarek, S. E., & Thornton, B. P. (2017). The effect of temperature on stoichiometry, cation ordering, and reaction rate in high-temperature dolomitization experiments. *Chemical Geology*, *468*(August), 32–41. https://doi.org/10.1016/j.chemgeo.2017.08.004

Kamber, B. S., Bolhar, R., & Webb, G. E. (2004). Geochemistry of late Archaean stromatolites from Zimbabwe: evidence for microbial life in restricted epicontinental seas. *Precambrian Research*, *132*(4), 379–399. https://doi.org/https://doi.org/10.1016/j.precamres.2004.03.006

Kısakürek, B., Eisenhauer, A., Böhm, F., Hathorne, E. C., & Erez, J. (2011). Controls on calcium isotope fractionation in cultured planktic foraminifera, Globigerinoides ruber and Globigerinella siphonifera. *Geochimica et Cosmochimica Acta*, *75*(2), 427–443.

Kozdon, R., Kelly, D. C., & Valley, J. W. (2018). Diagenetic Attenuation of Carbon Isotope Excursion Recorded by Planktic Foraminifers During the Paleocene-Eocene Thermal

Maximum. *Paleoceanography and Paleoclimatology*, *33*(4), 367–380. https://doi.org/10.1002/2017PA003314

De La Rocha, C. L., & DePaolo, D. J. (2000). Isotopic evidence for variations in the marine calcium cycle over the cenozoic. *Science*, *289*(5482), 1176–1178. https://doi.org/10.1126/science.289.5482.1176

Langer, G., Gussone, N., Nehrke, G., Riebesell, U., Eisenhauer, A., & Thoms, S. (2007). Calcium isotope fractionation during coccolith formation in Emiliania huxleyi: Independence of growth and calcification rate. *Geochemistry, Geophysics, Geosystems*, *8*(5), 1–11. https://doi.org/10.1029/2006GC001422

Lemarchand, D., Wasserburg, G. J., & Papanastassiou, D. A. (2004). Rate-controlled calcium isotope fractionation in synthetic calcite. *Geochimica et Cosmochimica Acta*, *68*(22), 4665–4678. https://doi.org/10.1016/j.gca.2004.05.029

Li, W., Beard, B. L., Li, C., Xu, H., & Johnson, C. M. (2015). Experimental calibration of Mg isotope fractionation between dolomite and aqueous solution and its geological implications. *Geochimica et Cosmochimica Acta*, *157*, 164–181. https://doi.org/10.1016/j.gca.2015.02.024

Lowenstein, T. K., Hardie, L. A., Timofeeff, M. N., & Demicco, R. V. (2003). Secular variation in seawater chemistry and the origin of calcium chloride basinal brines. *Geology*, *31*(10), 857–860. https://doi.org/10.1130/G19728R.1

Lü, C., Wu, S., Yao, Y., & Fulthorpe, C. S. (2013). Development and controlling factors of Miocene carbonate platform in the Nam Con Son Basin, southwestern South China Sea. *Marine and Petroleum Geology*, *45*, 55–68. https://doi.org/10.1016/j.marpetgeo.2013.04.014

Mathew, M., Makhankova, A., Menier, D., Sautter, B., Betzler, C., & Pierson, B. (2020). The emergence of Miocene reefs in South China Sea and its resilient adaptability under varying eustatic, climatic and oceanographic conditions. *Scientific Reports*, *10*(1), 1–16. https://doi.org/10.1038/s41598-020-64119-9

McArthur, J. M., Howarth, R. J., & Shields, G. A. (2012). Strontium isotope stratigraphy. *The Geologic Time Scale*, *1*, 96–105. https://doi.org/10.1017/CBO9780511536045.008

Melim, L. A., Westphal, H., Swart, P. K., Eberli, G. P., & Munnecke, A. (2002). Questioning carbonate diagenetic paradigms: evidence from the Neogene of the Bahamas. *Marine Geology*, *185*(1), 27–53. https://doi.org/https://doi.org/10.1016/S0025-3227(01)00289-4

Meyers, W. J., Lu, F. H., & Zachariah, J. K. (1997). Dolomitization by mixed evaporative brines and freshwater, upper Miocene carbonates, Nijar, Spain. *Journal of Sedimentary Research*, *67*(5), 898–912. https://doi.org/10.1306/D4268671-2B26-11D7-8648000102C1865D

Milliman, J. D., & Droxler, A. W. (1996). Neritic and pelagic carbonate sedimentation in the marine environment: Ignorance is not bliss. *International Journal of Earth Sciences*, *85*(3), 496–504. https://doi.org/10.1007/s005310050090

Misra, S., & Froelich, P. N. (2012). Lithium isotope history of cenozoic seawater: Changes in silicate weathering and reverse weathering. *Science*, *335*(6070), 818–823. https://doi.org/10.1126/science.1214697

Nielsen, L. C., DePaolo, D. J., & De Yoreo, J. J. (2012). Self-consistent ion-by-ion growth model for kinetic isotopic fractionation during calcite precipitation. *Geochimica et Cosmochimica Acta*, *86*, 166–181. https://doi.org/10.1016/j.gca.2012.02.009

Pleydell, S. M., Jones, B., Longstaffe, F. J., & Baadsgaard, H. (1990). Dolomitization of the Oligocene–Miocene Bluff Formation on Grand Cayman, British West Indies. *Canadian Journal of Earth Sciences*, *27*(8), 1098–1110. https://doi.org/10.1139/e90-114

Raymo, M. E., & Ruddiman, W. F. (1992). Tectonic forcing of late Cenozoic climate. *Nature*, *359*(6391), 117–122.

Ren, M., & Jones, B. (2017). Spatial variations in the stoichiometry and geochemistry of Miocene dolomite from Grand Cayman: Implications for the origin of island dolostone. *Sedimentary Geology*, *348*, 69–93. https://doi.org/10.1016/j.sedgeo.2016.12.001

Roberts, J., Kaczmarek, K., Langer, G., Skinner, L. C., Bijma, J., Bradbury, H., et al. (2018). Lithium isotopic composition of benthic foraminifera: A new proxy for paleo-pH reconstruction. *Geochimica et Cosmochimica Acta*, *236*, 336–350. https://doi.org/10.1016/j.gca.2018.02.038

Royse, C. F., Wadell, J. S., & Petersen, L. E. (1971). X-ray determination of calcite-dolomite; an evaluation. *Journal of Sedimentary Research*, *41*(2), 483–488. https://doi.org/10.1306/74D722A7-2B21-11D7-8648000102C1865D

Schmitt, A.-D. D., Stille, P., & Vennemann, T. (2003). Variations of the 44Ca/40Ca ratio in seawater during the past 24 million years: Evidence from δ44Ca and δ18O values of Miocene phosphates. *Geochimica et Cosmochimica Acta*, *67*(14), 2607–2614. https://doi.org/10.1016/S0016-7037(03)00100-5

Schmitt, A. D., Chabaux, F., & Stille, P. (2003). The calcium riverine and hydrothermal isotopic fluxes and the oceanic calcium mass balance. *Earth and Planetary Science Letters*, *213*(3–4), 503–518. https://doi.org/10.1016/S0012-821X(03)00341-8

Shao, L., Cui, Y., Qiao, P., Zhang, D., Liu, X., & Zhang, C. (2017). Sea-level changes and carbonate platform evolution of the Xisha Islands (South China Sea) since the Early Miocene. *Palaeogeography, Palaeoclimatology, Palaeoecology*, *485*, 504–516. https://doi.org/10.1016/j.palaeo.2017.07.006

Sime, N. G., De La Rocha, C. L., Tipper, E. T., Tripati, A., Galy, A., & Bickle, M. J. (2007). Interpreting the Ca isotope record of marine biogenic carbonates. *Geochimica et Cosmochimica Acta*, *71*(16), 3979–3989. https://doi.org/https://doi.org/10.1016/j.gca.2007.06.009

Skulan, J., DePaolo, D. J., & Owens, T. L. (1997). Biological control of calcium isotopic abundances in the global calcium cycle. *Geochimica et Cosmochimica Acta*, *61*(12), 2505–2510. https://doi.org/10.1016/S0016-7037(97)00047-1

Swart, P. K. (2015). The geochemistry of carbonate diagenesis: The past, present and future. *Sedimentology*, *62*(5), 1233–1304. https://doi.org/10.1111/sed.12205

Tang, J., Dietzel, M., Böhm, F., Köhler, S. J., & Eisenhauer, A. (2008). Sr2+/Ca2+ and 44Ca/40Ca fractionation during inorganic calcite formation: II. Ca isotopes. *Geochimica et Cosmochimica Acta*, *72*(15), 3733–3745. https://doi.org/10.1016/j.gca.2008.05.033

Tipper, E. T., Schmitt, A. D., & Gussone, N. (2016). *Global Ca Cycles: Coupling of Continental and Oceanic Processes*. *Advances in Isotope Geochemistry*. https://doi.org/10.1007/978-3-540-68953-9_6

Tostevin, R., Bradbury, H. J., Shields, G. A., Wood, R. A., Bowyer, F., Penny, A. M., & Turchyn, A. V. (2019). Calcium isotopes as a record of the marine calcium cycle versus carbonate diagenesis during the late Ediacaran. *Chemical Geology*, *529*, 119319. https://doi.org/10.1016/j.chemgeo.2019.119319

Urey, H. C. (1952). The Planets: Their Origin and Development. *Yale University Press*.

Wallmann, K. (2001). Controls on the Cretaceous and Cenozoic evolution of seawater composition, atmospheric CO2 and climate. *Geochimica et Cosmochimica Acta*, *65*(18), 3005–3025. https://doi.org/10.1016/S0016-7037(01)00638-X

Wang, C., He, X., & Qiu, S. (1979). A preliminary study on carbonate stratigraphy and micropalaeontology of well Xiyong-1, Xisha Islands. *Petroleum Geology and Experiment*, (00), 23–38, 73.

Wang, Z., Shi, X., Yang, J., Huang, B., Sun, Z., Wang, Y., et al. (2014). Analyses on the tectonic thermal evolution and influence factors in the deep-water Qiongdongnan Basin. *Acta Oceanologica Sinica*, *33*(12), 107–117. https://doi.org/10.1007/s13131-014-0580-9

Wang, Z., Huang, K., Zhang, D., You, L., Liu, X., & Luo, W. (2018). Maturation of Neogene dolomite from Xuande Atoll of Xisha archipelago, the South China Sea. *Marine and Petroleum Geology*, *92*, 51–64. https://doi.org/10.1016/j.marpetgeo.2018.02.016

Wanner, C., Sonnenthal, E. L., & Liu, X.-M. M. (2014). Seawater δ7Li: A direct proxy for global CO2 consumption by continental silicate weathering? *Chemical Geology*, *381*, 154–167. https://doi.org/10.1016/j.chemgeo.2014.05.005

Wilkinson, B. H., & Walker, J. C. G. (1989). Phanerozoic cycling of sedimentary carbonate. *American Journal of Science*, *289*(4), 525–548.

Wu, F., Xie, X., Li, X., Betzler, C., Shang, Z., & Cui, Y. (2019). Carbonate factory turnovers influenced by the monsoon (Xisha Islands, South China Sea). *Journal of the Geological Society*, *176*(5), 885–897. https://doi.org/10.1144/jgs2018-086

Wu, S., Yang, Z., Wang, D., Lü, F., Lüdmann, T., Fulthorpe, C., & Wang, B. (2014). Architecture, development and geological control of the Xisha carbonate platforms, northwestern South China Sea. *Marine Geology*, *350*, 71–83. https://doi.org/10.1016/j.margeo.2013.12.016

Wu, S., Zhang, X., Yang, Z., Wu, T., Gao, J., & Wang, D. (2016). Spatial and temporal evolution of Cenozoic carbonate platforms on the continental margins of the South China Sea: Response to opening of the ocean basin. *Interpretation*, *4*(3), SP1–SP19. https://doi.org/10.1190/INT-2015-0162.1

Xiu, C., Zhang, D., Zhai, S., Liu, X., & Bi, D. (2016). Zricon U-Pb age of granitic rocks from the basement beneath the Shi Island, Xisha Islands and its geological significance. *Marine Geology & Quaternary Geology*, *36*(3), 115–126.

Yi, L., Jian, Z., Liu, X., Zhu, Y., Zhang, D., Wang, Z., & Deng, C. (2018). Astronomical tuning and magnetostratigraphy of Neogene biogenic reefs in Xisha Islands, South China Sea. *Science Bulletin*, *63*(9), 564–573. https://doi.org/10.1016/j.scib.2018.04.001

Yu, J., Menviel, L., Jin, Z. D., Anderson, R. F., Jian, Z., Piotrowski, A. M., et al. (2020). Last glacial atmospheric CO2 decline due to widespread Pacific deep-water expansion. *Nature Geoscience*, *13*(9), 628–633. https://doi.org/10.1038/s41561-020-0610-5

Zhai, S., Mi, L., Shen, X., Liu, X., Xiu, C., Sun, Z., & Cao, J. (2015). Mineral compositions and their environmental implications in reef of Shidao Island, Xisha. *Earth Science-Journal of China University of Geosciences*, *40*, 597–605. Retrieved from in Chinese with English abstract

Zhao, Q. (2010). *The Sedimentary Research about Reef Carbonate in Xisha Islands Waters*. Chinese Academy of Sciences.

Zhu, P., & Douglas Macdougall, J. (1998). Calcium isotopes in the marine environment and the oceanic calcium cycle. *Geochimica et Cosmochimica Acta*. https://doi.org/10.1016/S0016-7037(98)00110-0

Zhu, W. L., Xie, X. N., Wang, Z. F., Zhang, D. J., Zhang, C. L., Cao, L. C., & Shao, L. (2017). New insights on the origin of the basement of the Xisha Uplift, South China Sea. *Science China Earth Sciences*, *60*(12), 2214–2222. https://doi.org/10.1007/s11430-017-9089-9